

## Noncovalent Mutant Selective Epidermal Growth Factor Receptor Inhibitors: A Lead Optimization Case History

Robert Andrew Heald, Bryan K Chan, 2. Callie Bryan, Charles Eigenbrot, Christine Yu, Daniel Burdick, Emily J. Hanan, Emily Chan, Gabriele Schaefer, Hank La, Hans Purkey, Jamie Knight, Ivana Yen, Philip Jackson, Krista Bowman, Kyle Mortara, Michael Lainchbury, Lily Shao, Richard Elliott, Eileen Seward, Shiva Malek, Stephen Schmidt, Steve Sideris, Timothy P Heffron, Kuen Yeap, Yuan Chen, and Sam Mann

*J. Med. Chem.*, **Just Accepted Manuscript** • Publication Date (Web): 10 Oct 2015

Downloaded from <http://pubs.acs.org> on October 11, 2015

### Just Accepted

“Just Accepted” manuscripts have been peer-reviewed and accepted for publication. They are posted online prior to technical editing, formatting for publication and author proofing. The American Chemical Society provides “Just Accepted” as a free service to the research community to expedite the dissemination of scientific material as soon as possible after acceptance. “Just Accepted” manuscripts appear in full in PDF format accompanied by an HTML abstract. “Just Accepted” manuscripts have been fully peer reviewed, but should not be considered the official version of record. They are accessible to all readers and citable by the Digital Object Identifier (DOI®). “Just Accepted” is an optional service offered to authors. Therefore, the “Just Accepted” Web site may not include all articles that will be published in the journal. After a manuscript is technically edited and formatted, it will be removed from the “Just Accepted” Web site and published as an ASAP article. Note that technical editing may introduce minor changes to the manuscript text and/or graphics which could affect content, and all legal disclaimers and ethical guidelines that apply to the journal pertain. ACS cannot be held responsible for errors or consequences arising from the use of information contained in these “Just Accepted” manuscripts.

# Noncovalent Mutant Selective Epidermal Growth Factor Receptor Inhibitors: A Lead Optimization Case Study

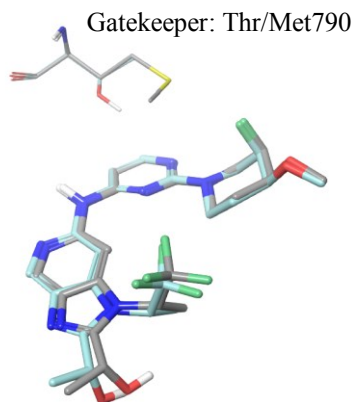
*Robert Heald,<sup>\*Δ</sup> Krista K. Bowman,<sup>±</sup> Marian C. Bryan,<sup>†</sup> Daniel Burdick,<sup>†</sup> Bryan Chan,<sup>†</sup> Emily Chan,<sup>□</sup> Yuan Chen,<sup>§</sup> Sandra Clausen,<sup>◇</sup> Charles Eigenbrot,<sup>‡</sup> Richard Elliott,<sup>Δ</sup> Emily J. Hanan,<sup>†</sup> Philip Jackson,<sup>Δ</sup> Jamie Knight,<sup>Δ</sup> Hank La,<sup>§</sup> Michael Lainchbury,<sup>Δ</sup> Shiva Malek,<sup>◇</sup> Sam Mann,<sup>Δ</sup> Mark Merchant,<sup>□</sup> Kyle Mortara,<sup>±</sup> Hans Purkey,<sup>†</sup> Gabriele Schaefer,<sup>#</sup> Stephen Schmidt,<sup>◇</sup> Eileen Seward,<sup>Δ</sup> Steve Sideris,<sup>◇</sup> Lily Shao,<sup>□</sup> Shumei Wang,<sup>†</sup> Kuen Yeap,<sup>Δ</sup> Ivana Yen,<sup>◇</sup> Christine Yu,<sup>‡</sup> Timothy P. Heffron<sup>†</sup>*

<sup>Δ</sup>Argenta, Early Discovery Charles River, 7/9 Spire Green Centre, Flex Meadow, Harlow, Essex CM19 5TR, United Kingdom. <sup>†</sup>Departments of Discovery Chemistry, <sup>‡</sup>Structural Biology, <sup>§</sup>Drug Metabolism and Pharmacokinetics, <sup>◇</sup>Biochemical and Cellular Pharmacology, <sup>#</sup>Molecular Oncology, <sup>□</sup> Research Oncology and <sup>±</sup>Protein Expression Genentech Inc., 1 DNA Way, South San Francisco, California, 94080, United States.

Due to their increased activity against activating mutants, first-generation epidermal growth factor receptor (EGFR) kinase inhibitors have had remarkable success in treating non-small cell lung cancer (NSCLC) patients, but acquired resistance, through a secondary mutation of the gatekeeper residue, means that clinical responses only last for 8-14 months. Addressing this

1  
2  
3 unmet medical need requires agents which can target both of the most common double mutants:  
4  
5 T790M/L858R (TMLR) and T790M/del(746-750) (TMdel). Herein we describe how a  
6  
7  
8 noncovalent double-mutant selective lead compound was optimized using a strategy focused on  
9  
10 the structure-guided increase in potency without added lipophilicity or reduction of 3-  
11  
12 dimensional character. Following successive rounds of design and synthesis it was discovered  
13  
14 that cis-fluoro substitution on 4-hydroxy and 4-methoxy piperidinyl groups provided synergistic,  
15  
16 substantial, and specific potency gain either through direct interaction with the enzyme and/or  
17  
18 effects on the proximal ligand oxygen atom. Further development of the fluoro-hydroxy  
19  
20 piperidine series resulted in the identification of a pair of diastereomers which showed 50-fold  
21  
22 enzyme and cell based selectivity for T790M mutants over wild-type EGFR (wtEGFR) in vitro  
23  
24 and pathway knock-down in an in vivo xenograft model.  
25  
26  
27  
28  
29

### 30 GRAPHICAL ABSTRACT



Identical wtEGFR (cyan) and T790M/ L858R (gray) binding modes,  
>100-fold enzyme and cell selectivity.

## INTRODUCTION

Activating mutations of the receptor tyrosine kinase epidermal growth factor receptor (EGFR), most commonly the point mutation L858R or deletions within exon 19, increase EGFR-driven cell proliferation and survival<sup>1-4</sup> leading to oncogene addiction in non-small cell lung cancer (NSCLC) bearing these mutations.<sup>5</sup> Successful treatment of EGFR-mutated NSCLC with erlotinib or gefitinib<sup>6-10</sup> is followed in most cases by acquired resistance to the respective TKI (tyrosine-kinase inhibitor).<sup>11-13</sup> In particular, around 60% of patients acquire a secondary mutation of the gatekeeper residue threonine-790 to methionine (T790M).<sup>12-16</sup> This mutation maintains catalytic function of the enzyme but reduces the activity of inhibitors gefitinib and erlotinib through occlusion of part of the binding site<sup>17</sup> similarly to the T315I gatekeeper residue resistance mutation in Abl following treatment with TKIs in CML.<sup>12, 13, 18-20</sup> A second mechanism, in which the T790M containing mutants have an increased affinity for ATP, resulting in reduced cellular potency for the ATP-competitive inhibitors has also been discovered.<sup>21</sup>

The predominant strategy employed by medicinal chemists to overcome these resistance mechanisms has been the use of covalent inhibitors which are able to bond with the poorly conserved Cys797 within the EGFR active site, providing both potency and kinase-selectivity. Clinical results with these second and third-generation compounds have been mixed. Clinical efficacy of second-generation EGFR inhibitors containing reactive groups was limited by associated skin rash and gastrointestinal toxicity, possibly because of their potency against wild-type EGFR (wtEGFR).<sup>22, 23</sup> These results and additional reports of acquired resistance to one such covalent inhibitor via the T790M mutation<sup>24, 25</sup> led to concerns that drug levels sufficient to inhibit T790M mutant forms of EGFR may not be achieved with these agents. Recent results

1  
2  
3 (disclosed after the conclusion of this work) for third-generation covalent inhibitors AZD9291  
4 (mereletinib) and CO-1686 (rociletinib), which have been designed to be selective for T790M  
5 containing EGFR mutants over wtEGFR, indicate promising efficacy and tolerability with this  
6 approach.<sup>26-33</sup> However, as with first and second-generation compounds, resistance has emerged:  
7 there has been a recent report of C797S mutation or loss of the T790M mutation in cell-free  
8 plasma DNA samples from patients who have developed resistance<sup>34</sup> and a second separate  
9 report of C797S mutation in biopsy samples from a single patient.<sup>35</sup> Additionally, studies with  
10 third-generation resistant cell lines have shown that the allelic context of the activating  
11 gatekeeper and C797S mutations affects the sensitivity to the three generations of inhibitors with  
12 no EGFR TKIs alone or in combination able to suppress activity when the mutations are in cis.<sup>36</sup>  
13 These data suggest that there is a need for drugs which do not rely on covalent reaction with  
14 Cys797 for potency or selectivity. The dual ALK/EGFR inhibitor AP26113 (brigatinib) is one of  
15 the few noncovalent EGFR T790M selective inhibitors to be resported<sup>37</sup> although the primary  
16 focus of clinical investigation appears to be in ALK (anaplastic lymphoma kinase) driven lung  
17 cancers.<sup>38</sup>

18  
19  
20  
21  
22  
23  
24  
25  
26  
27  
28  
29  
30  
31  
32  
33  
34  
35  
36  
37  
38  
39 Our previous publication<sup>39</sup> describes the first stage of our work to identify noncovalent  
40 mutant-selective inhibitors of the major resistant mutants of EGFR: T790M/L858R (TMLR) and  
41 T790M/del(746-750) (TMdel), with high selectivity over wtEGFR. Using structure-based  
42 design following an HTS campaign a novel series of pyrimidinyl-pyridines which offer  
43 selectivity for inhibition of TMLR and TMdel over wtEGFR and kinases in general were  
44 discovered. This selectivity is due to an unusual binding mode (**1**, Figure 1) where the  
45 pyrimidine ring sits underneath the mutated Met790 gatekeeper residue. Methionine-aryl  
46 interactions are frequently observed in protein structures with the methionine sulfur often found  
47  
48  
49  
50  
51  
52  
53  
54  
55  
56  
57  
58  
59  
60

1  
2  
3 to be positioned in the same plane as the aryl ring.<sup>40</sup> Additionally, the binding sites of adenine  
4 rings often feature methionine residues with the sulfur above the plane of the aromatic ring at a  
5 distance of  $\sim 4\text{\AA}$ , as exemplified in the complex of catechol-O-methyltransferase with its cofactor  
6 S-adenosylmethionine (PDB code 2cl5). The Met790 gatekeeper residue of the TMLR enzyme  
7 and pyrimidine ring of **1** are in a similar juxtaposition (Figure 1c). The pyrimidine ring is also  
8 held in place through a hydrogen bond with the non-conserved Thr854 residue. This residue, or  
9 a corresponding hydrogen bond donor is unusual in combination with a methionine gatekeeper.<sup>41</sup>  
10 The methoxy piperidine, which was found to be key to selectivity and stabilization of this  
11 binding mode, fills the lipophilic space between Met790 and Lys745 placing the ether oxygen, a  
12 weak hydrogen-bond acceptor, within hydrogen-bonding distance with the conserved catalytic  
13 lysine (Figure 1). Successful X-ray refinement places the methoxyl oxygen in the preferred  
14 equatorial conformation, while the methoxyl methyl carbon is less strongly indicated. The  
15 aminopyridine core makes two additional hydrogen-bonding interactions with the hinge, with the  
16 pyrimidine CH also within close contact with the carbonyl oxygen of Gln791. Finally, the *N*-  
17 substituent on the ring fused to the pyridine (imidazole in the case of **1**) fills the lipophilic ribose  
18 pocket formed by Val726, Leu844 and Cys797. A cysteine residue in this position in the ribose  
19 pocket is unusual in kinases so although the interactions of this group are lipophilic this may still  
20 contribute to selectivity.  
21  
22  
23  
24  
25  
26  
27  
28  
29  
30  
31  
32  
33  
34  
35  
36  
37  
38  
39  
40  
41  
42  
43  
44  
45  
46  
47  
48  
49  
50  
51  
52  
53  
54  
55  
56  
57  
58  
59  
60

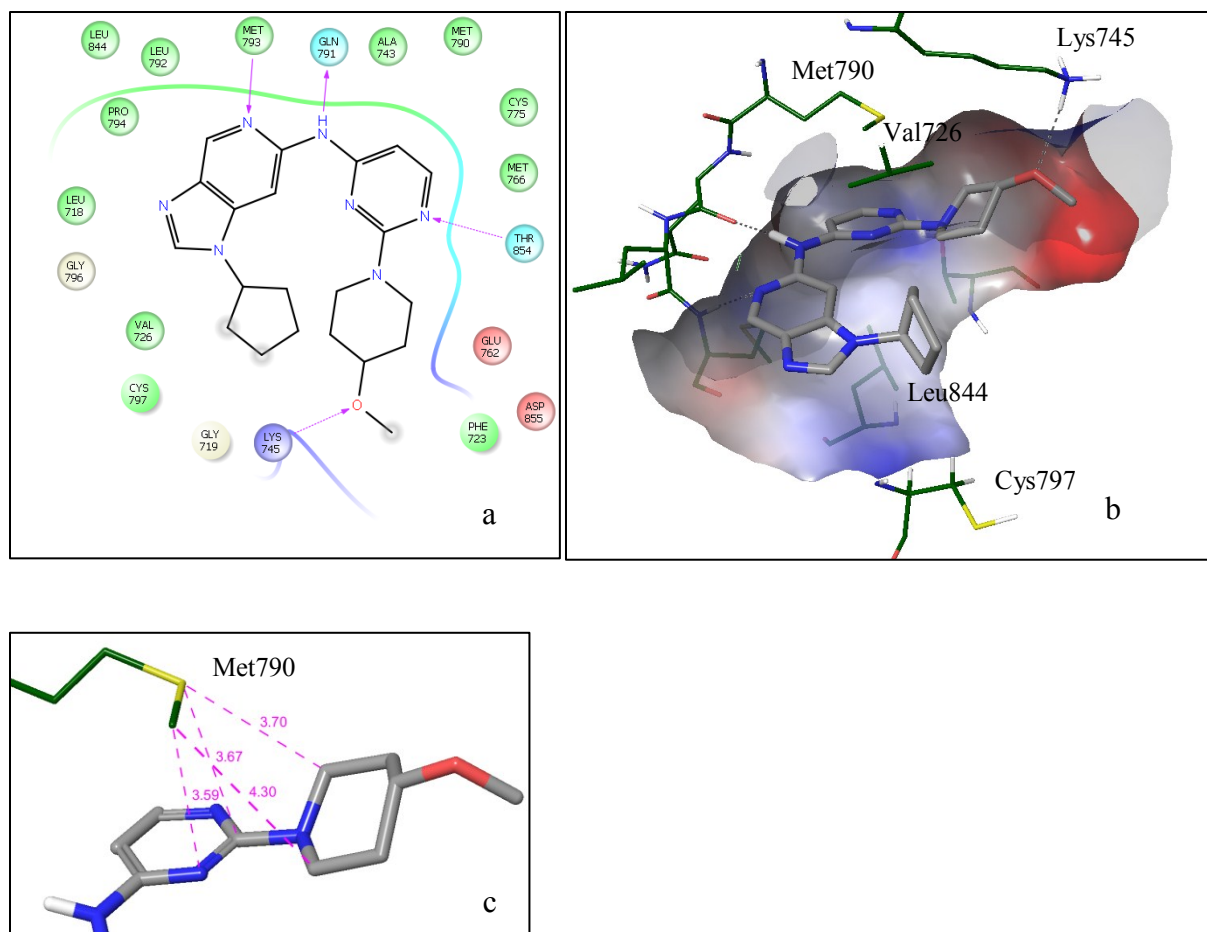


**Figure 1.** Representations of the X-ray structure of **1** complexed with TMLR (PDB code 5C8K). Some residues removed for clarity. a) Chemical structure of **1** and interaction map with TMLR, purple arrows indicate hydrogen bonds; b) overview of **1** in the binding site, the surface shown is colored by electrostatic potential, hydrogen bonds indicated by dashed gray lines; c) close-in image showing the position of the pyrimidine and piperidine rings relative to the mutated gatekeeper residue, inter-atom distances for the methionine gatekeeper sulfur and heavy atoms of the pyrimidine ring and piperidine and shown by dashed purple lines, values in Å.

It is generally accepted that with increasing lipophilicity (LogP) the *risk* of promiscuous binding and toxicity is increased, and metabolic stability and solubility are reduced.<sup>42,43</sup> Similar relationships have been postulated to exist with reduced 3-dimensional character<sup>44</sup> and increased

1  
2  
3 aromatic ring count.<sup>45</sup> These risk factors were anticipated to be a particular challenge in our  
4  
5 optimization program for a number of reasons:  
6  
7

- 8  
9 1. The EGFR ATP binding-site is surrounded by mostly lipophilic residues, reflected in the  
10 highly lipophilic nature of optimized compounds erlotinib and gefitinib (clogP 3.8, 4.3;  
11 measured Log D 3.1, 3.6 respectively). In T790M EGFR lipophilicity is increased by  
12 substitution of the only H-bonding residue used by quinazoline inhibitors (excluding  
13 hinge interactions) T790 with methionine.  
14  
15
- 16 2. The binding site occupied by our lead compounds is flatter than in the case of anilino-  
17 quinazoline EGFR inhibitors where the aryl ring sits out of plane and is orientated  
18 towards the gatekeeper pocket (see pdb entry 1M17).  
19  
20
- 21 3. Achieving cellular potency and selectivity is made more difficult by the low  $K_M$ [ATP] of  
22 T790M mutant EGFR ( $TMLR = 1.3 \mu M$ ,  $TMdel = 2.1 \mu M$ <sup>46</sup>), compared to many other  
23 kinases. Literature values for  $K_M$ [ATP] vary significantly although it is generally  
24 accepted that the activating mutations have increased  $K_M$  compared to wtEGFR and  
25 T790M kinases.  
26  
27  
28  
29  
30  
31  
32  
33  
34  
35  
36  
37  
38  
39  
40  
41  
42

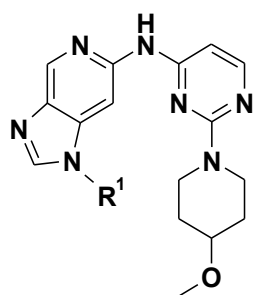
43 There is much discussion in the medicinal chemistry literature about the correlation of  
44 lipophilic ligand efficiency (LLE) with “compound quality” and the use of this and similar  
45 metrics in lead optimization programs.<sup>47-50</sup> Due to the particular challenges envisaged with the  
46 optimization of our series of T790M EGFR inhibitors and centered on the thermodynamic basis  
47 for the use of lipophilic efficiency in optimizing enthalpic contributions to potency<sup>51</sup> our strategy  
48 was to analyze potency in the context of measured LogD values. This was in order to avoid  
49 hydrophobic-effect driven potency increases which may well be non-selective and lead to  
50  
51  
52  
53  
54  
55  
56  
57  
58  
59  
60

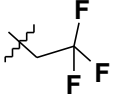
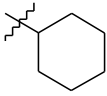
1  
2  
3 ADMET issues. In concert with this we sought to retain, or add to, the 3-dimensional character  
4 present in lead compounds. Finally, we made structural changes which removed metabolic soft  
5 spots identified in in vitro and in vivo studies focusing on increasing in vitro metabolic stability  
6 and lowering unbound in vivo clearance.  
7  
8  
9  
10  
11

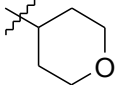
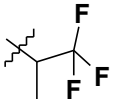
## 12 13 14 RESULTS AND DISCUSSION

15  
16  
17 The azabenzimidazole sub-series was chosen over other 5,6- and 6,6- systems due to superior  
18 physicochemical properties, chiefly solubility. Initially we carried out a survey of the effect of  
19 the azabenzimidazole *N*-substituent changes on enzyme affinity (Table 1). The TMLR enzyme  
20 assay alone was used primarily for optimization as a very strong correlation was found for  
21 TMLR vs TMdel affinity. Generally, the potency of these analogues correlated with  
22 lipophilicity, which could be expected based on the lipophilic nature of the ribose pocket.  
23 Ligand efficiency was retained in comparison with the unsubstituted analogue **2**. The isopropyl  
24 group appeared near-optimal at this stage and was retained in the preparation of further  
25 analogues due to the combination of good potency and LE but without excessive lipophilicity  
26 (LogD) and the absence of a chiral center.  
27  
28  
29  
30  
31  
32  
33  
34  
35  
36  
37  
38  
39  
40  
41

42 **Table 1.** TMLR enzyme potency of azabenzimidazole *N*-substituent analogues. Ent 1 and Ent 2  
43 denote separated single unknown stereoisomers.  
44  
45



compd	R <sup>1</sup>	TMLR LLE/LE <sup>a</sup>	TMLR K <sub>i</sub> <sub>app</sub> (nM)	LogD
1		4.8/0.36	20	2.9
2	H	4.6/0.37	329	1.9
3		4.3/0.35	201	2.4
4		4.8/0.36	87	2.3
5		4.9/0.38	40	2.5
6		4.5/0.36	48	2.8
7 (racemic)		5.1/0.38	14	2.8
8 (ent 1)		4.8/0.38	17	2.9
9 (ent 2)		4.8/0.38	22	2.9
10		5.0/0.32	149	1.8
11		4.3/0.34	71	2.8
12		4.3/0.35	18	3.4

13		5.0/0.33	76	2.1
14		4.9/0.35	27	2.7

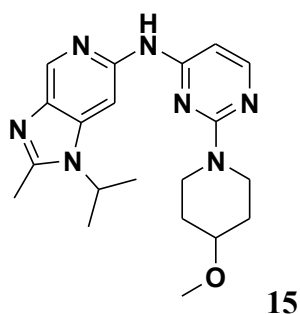
<sup>a</sup> LLE was calculated using measured LogD; Ligand efficiency,  $LE = (\Delta G)/N$  where N is the number of non-hydrogen atoms. Wavy line indicates the point of attachment to the imidazole N. See experimental section for details of assay errors and controls.

Compound **5** was profiled fully and found to be labile in liver microsomes and hepatocytes across species (human and rat liver microsomal  $Cl_{hep}$  15 and 44 mL/min/kg respectively) and also in the absence of co-factor (NADPH) in human liver microsomes ( $Cl_{hep}$  9 mL/min/kg). Incubation of a number of compounds in this series in human liver cytosol in the absence of co-factor (NADPH) showed disappearance of parent and the formation of an oxidative (M+16) metabolite. These data indicated likely involvement of non-CYP mediated oxidation through an enzyme such as aldehyde oxidase (AO) / xanthine oxidase (XO). AO and XO are known to metabolize various heterocycles, mainly at CH next to  $sp^2$  ring nitrogen atoms.<sup>52</sup> From the binding mode of this series we anticipated that only the azabenzimidazole 2-position could tolerate substitution with a methyl group without loss of activity. Encouragingly, **15**, the 2-methyl analogue of **5** (Table 2) showed a modest increase in potency and >10-fold selectivity for inhibition of EGFR auto-phosphorylation in the TMLR-expressing cell line H1975 over the wtEGFR cell line H292. Furthermore, **15** showed no loss of parent on incubation with cytosol as well as improved stability in human hepatocytes. In vivo clearance in rat was in line with that extrapolated from in vitro data<sup>53</sup> suggesting that in vivo clearance is mainly driven by hepatic metabolism and that PK for the series could be optimized through analysis of in vitro metabolic stability data. The major metabolites identified following incubation of **15** in human liver

microsomes were demethylation (M1, 26%), hydroxylation plus glucuronidation (M2, 10%) and hydroxylation plus glucuronidation of M1 (M3, 9%). The in vitro potency, ADME and rat PK profile of **15** are shown in Table 2.

Due to the clear metabolic liability of the methoxy piperidine and the probable weak hydrogen-bonding ability of the ether oxygen the piperidine substituent was targeted for optimization in the next round of synthesis. A number of simple analogues were prepared, focusing on removing the metabolic soft spot and including potentially stronger hydrogen bond acceptors in approximately the same position as the methoxy group. Data for four close analogues is shown in Table 3.

**Table 2.** In vitro potency, ADME and PK profile of **15**.

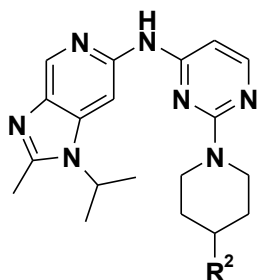


TMLR $K_{iapp}$ (nM)	19
wtEGFR $K_{iapp}$ (nM)	875
WT/TMLR $K_{iapp}$	46
p-EGFR/proliferation H1975 $IC_{50}/EC_{50}$ ( $\mu$ M)	0.882/ 6.7
p-EGFR H292 $IC_{50}$ ( $\mu$ M)	>10
Kinetic solubility ( $\mu$ M)	87
cLogP (measured LogD)	3.7 (2.4)
Microsomal $Cl_{hep}$ m/r/c/d/h <sup>a</sup> (mL/min/kg)	83/40/36/26/14

Hepatocyte $Cl_{\text{hep}}$ m/r/c/d/h <sup>a</sup> (mL/min/kg)	77/35/33/21/5
MDCK Papp A:B (x10 <sup>-6</sup> cm/s)	29
Rat IV (5 mg/kg) $Cl_p/Cl_u$ <sup>b</sup> (mL/min/kg)	40/620
F (10 mg/kg) %	30

<sup>a</sup> m: mouse; r: rat, d: dog, c: cynomolgus monkey h: human; <sup>b</sup>  $Cl_p$ : plasma clearance,  $Cl_u$ : unbound plasma clearance ( $Cl_p/F_u$  where  $F_u$  is the fraction unbound in plasma). Papp AB: apparent permeability, apical to basolateral; F: oral bioavailability. See experimental section for details of assay errors and controls.

**Table 3.** In vitro potency, LogD, and human in vitro metabolic stability for simple piperidine analogues.



compd	R <sup>2</sup>	TMLR K <sub>i,app</sub> (nM)	cLogP	LogD	LLE <sup>a</sup>	HLM/HH $Cl_{\text{hep}}$ (mL/min/kg)
<b>15</b>	OMe	19	3.7	2.4	5.3	14/5
<b>16</b>	OH	34	3.3	1.8	5.7	3/14
<b>17</b>	SO <sub>2</sub> Me	64	2.7	1.6	5.6	7/2
<b>18<sup>c</sup></b>	CONH <sub>2</sub>	151	2.2	1.7	5.1	8/-

<sup>a</sup> LLE was calculated using measured LogD; <sup>b</sup> HLM: human liver microsomes, HH: human hepatocytes; <sup>c</sup> 2-H azabenzimidazole scaffold. See experimental section for details of assay errors and controls.

The hydroxy piperidine analogue **16** was of comparable potency to **15**, and was much more stable in HLM (3 cf. 14 mL/min/kg). However, lower stability was observed in hepatocytes

1  
2  
3 presumably due to Phase II conjugation of the hydroxyl group of **16**. The piperidine sulfone  
4 analogue **17** was ~3-fold less potent but was more stable in both microsomes and hepatocytes.  
5  
6 The amide **18** lost >5-fold potency relative to the methyl ether **15**. The LLE values based on  
7  
8 measured LogD<sup>54</sup> indicate that both **16** and **17** represent a marginal improvement in  
9  
10 potency/lipophilicity balance. An X-ray structure of **17** in complex with the TMLR enzyme  
11  
12 (Figure 2a) showed Lys745 within hydrogen bonding distance of one of the sulfone oxygen  
13  
14 atoms, with this group in the more energetically favored equatorial conformation. The hydrogen  
15  
16 bond acceptor shifted ~1.4 Å compared to the methoxy piperidine analogue (Figure 2h) and the  
17  
18 lysine moves accordingly to accommodate this. The methyl group of the sulfone is also  
19  
20 positioned within interacting distance with Phe723 and Val726 (3.0 and 3.1 Å respectively).  
21  
22 Perhaps one reason for the lack of potency improvement with this substitution is that one of the  
23  
24 sulfone oxygen atoms is redundant making no clear contribution to binding.  
25  
26  
27  
28  
29  
30  
31  
32  
33  
34  
35  
36  
37  
38  
39  
40  
41  
42  
43  
44  
45  
46  
47  
48  
49  
50  
51  
52  
53  
54  
55  
56  
57  
58  
59  
60

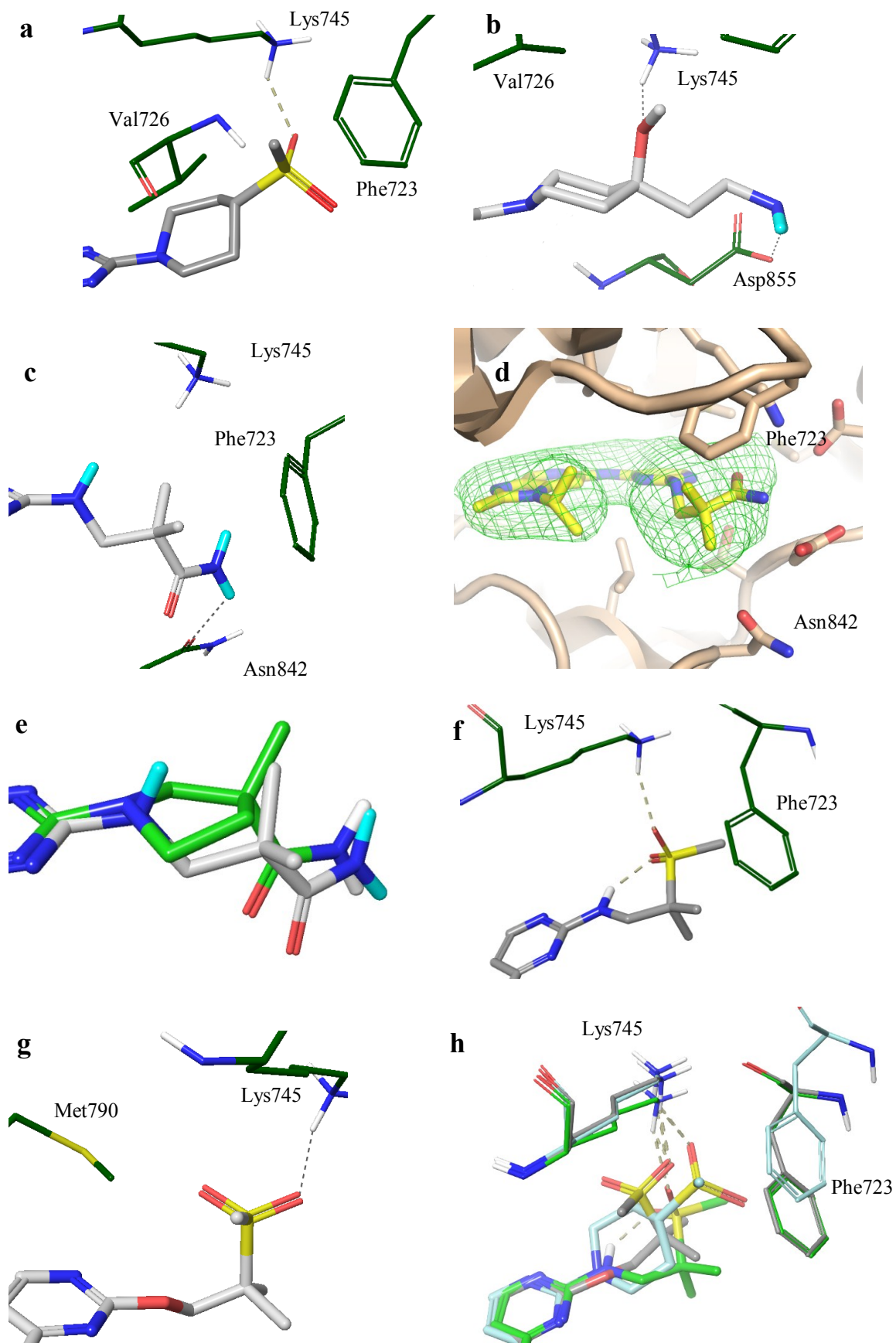
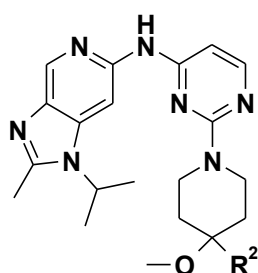


**Figure 2.** Representations of the X-ray structures of various piperidine-replacement analogues complexed with TMLR showing close-in images of the pyrimidine 2-substituent and key interacting residues. Hydrogen bonds are indicated by dashed gray lines. a) **17** (PDB code 5C8M). The sulfone is in the more stable equatorial conformation, hydrogen bond shown between Lys745 and one of the oxygen atoms of the sulfone, Phe723 is 3-3.2 Å from the methyl of the sulfone; b) **23** (PDB code 5C8N). The methoxy group is flipped to the axial conformation but is still able to interact with Lys745 through a hydrogen bond, the pendant amino group is able to make a salt bridge with Asp855; c) **24** (PDB code 5CAL). Image shown has the pendant group in the “open” conformation where there is no hydrogen bond with Lys745, the amide NH<sub>2</sub> is within hydrogen-bonding distance with Asn842, one of the methyl groups is positioned 3.7 Å from Phe723; d) hybrid fit of **24** to the X-ray electron density map, electron density shown in green e) **27** (green carbons) (PDB code 5CAN) in comparison with the ligand conformation of **24** (light gray carbons). The amide NH<sub>2</sub> is positioned so as to enable hydrogen bonding with Asn842 in both structures; f) **29** (PDB code 5CAO). The ligand bound conformation is possibly stabilized by an intramolecular hydrogen bond between the sulfone and aminopyrimidine NH; g) **30** (PDB code 5CAP). The O-linked analogue of **29**, where there is no intramolecular hydrogen bond with the sulfone, binds with the sulfone more out of plane but still interacting with Lys745; h) overlay of the X-ray structures of various pyrimidine substituent analogues (**17**, cyan; **29**, green and **30**, gray) showing the conservation in the positioning of the hydrogen bond acceptor and Lys745 in the complexes of these analogues.

4,4-Disubstituted quaternary piperidines **19-23** were designed to provide a steric block to metabolism of the methoxy piperidine or phase-II conjugation of the hydroxyl piperidine. Additionally these analogues also provided a vector for accessing polar interactions in particular

with Asp855 and Asn842. As shown in Table 4, two of these analogues, **21** and **23**, showed retention of potency with increased LLE indicating that the added polar groups, although sub-optimal, were achieving a positive interaction with the protein. Gratifyingly, compounds **21** and **23** also have improved HLM stability relative to compound **15** ( $Cl_{\text{hep}} = 2$  and 6 respectively compared to 14 mL/min/kg).

**Table 4.** In vitro potency, LogD, and human in vitro metabolic stability for quaternary piperidine analogues.



compd	R <sup>2</sup>	TMLR K <sub>i</sub> <sub>app</sub> (nM)	cLogP	LogD	LLE <sup>a</sup>	HLM/HH <sup>b</sup> Cl <sub>hep</sub> (mL/min/kg)
<b>19</b>	CH <sub>2</sub> N(Me) <sub>2</sub>	492	3.7	1.5	4.8	8/-
<b>20</b>	CH <sub>2</sub> OMe	77	3.6	2.4	4.7	14/-
<b>21</b>	CH <sub>2</sub> OH	24	3.0	1.7	5.9	6/10
<b>22</b>	CH <sub>2</sub> CH <sub>2</sub> OH	50	3.5	2.0	5.3	9/-
<b>23</b>	CH <sub>2</sub> CH <sub>2</sub> NH <sub>2</sub>	28	3.2	0.1	7.5 <sup>b</sup>	2/-

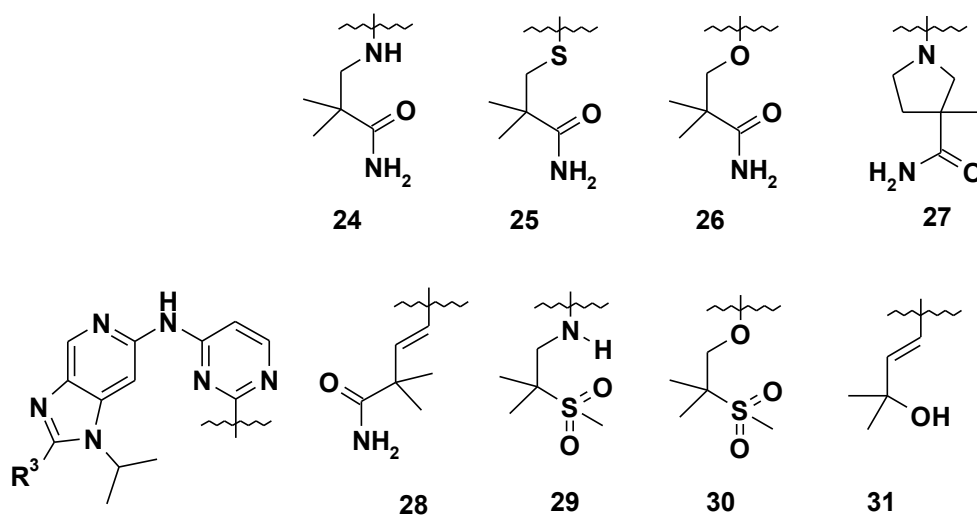
<sup>a</sup> LLE was calculated using measured LogD <sup>b</sup> HLM: human liver microsomes, HH: human hepatocytes. See experimental section for details of assay errors and controls.

The X-ray structure of **23** with TMLR (Figure 2b) showed that the basic primary amine is positioned within an appropriate distance to make a salt-bridge with Asp855. There is no potency gain with this interaction possibly due to an increased de-solvation penalty,

displacement of water which usually occupies this position and the fact that Asp855 is already part of a favorable hydrogen-bonding network in the apo enzyme. The X-ray structure also showed that **23** binds with the piperidine methoxy axial, now the preferred conformation due to the larger A-value of the ethyl amino group,<sup>55</sup> but the hydrogen bond with Lys745 is maintained.

A diverse library of >200 analogs varying the 2-substituent of the pyrimidine was prepared using commercially available primary and secondary amines. The amines were triaged using calculated property filters<sup>56</sup> in an empirically-driven approach to identify a replacement for the methoxypiperidine moiety which conferred improved metabolic stability and comparable potency. The vast majority of these analogues were substantially less potent than the methoxy piperidine (data not shown) with only one compound showing activity < 30 nM, **24**, Table 5. This analogue was significantly more polar than **15** (LogD lowered by 0.8 units), devoid of an obviously metabolically labile group on the amino pyrimidine, and had improved stability in liver microsomes and hepatocytes.

**Table 5.** In vitro potency, LogD, and human in vitro metabolic stability for library analogue **24** and related compounds.



compd	R <sup>3</sup>	TMLR Kiapp (nM)	wtEGFR Kiapp (nM)	cLogP	LogD	LLE <sup>a</sup>	HLM/HH <sup>b</sup> Cl <sub>hep</sub> (mL/min/kg)
<b>24</b>	Me	22	390	2.4	1.5	6.2	5/3
<b>25</b>	Me	658	>2500	3.0	1.9	4.3	7/-
<b>26</b>	H	196	>440	2.1	1.6	5.1	4/-
<b>27</b>	Me	124	681	2.3	1.6	5.3	4/5
<b>28</b>	Me	196	>1500	3.3	2.2	4.5	5/<1
<b>29</b>	Me	38	1820	2.0	1.4	6.0	5/6
<b>30</b>	Me	52	2100	2.1	1.6	5.9	4/1
<b>31</b>	Me	323	>2500	2.8	2.0	4.5	5/2

<sup>a</sup>LLE calculated using measured LogD <sup>b</sup> HLM: human liver microsomes, HH: human hepatocytes. See experimental section for details of assay errors and controls.

The bound conformation of **24** as determined by X-ray showed the N-linked side chain in an “extended” conformation (Figure 2c), but an alternate fit to the electron density showed a “closed” conformation (Figure 2d). In the extended conformation the amide NH<sub>2</sub> is able to hydrogen bond with Asn842 and the carbonyl appears redundant. In the closed conformation the amide carbonyl is positioned within hydrogen-bonding distance with Lys745 and the amide NH<sub>2</sub> makes no discernable interaction. It is likely that the closed conformation of **24** is the preferred small molecule conformation due to an intramolecular hydrogen bond between the carbonyl and NH and the Thorpe-Ingold effect, but both bound conformations may contribute to potency. The S- and O- linked compounds **25** and **26** are likely to exist in the extended ligand conformation in solution due to the absence of a strong intramolecular H-bond and the propensity for O- and S- linked side chains to sit out of plane with the pyrimidine core. Both analogues are less potent than **24** suggesting that the closed conformation predominates in this compound and provides greater potency. Supporting this, docking of **24** in the receptor from its

own X-ray using GLIDE provides a closed binding conformation as the highest scoring result. Competition between the two binding conformations was further illuminated following the serendipitous synthesis (see synthesis section below for details) of **27**. This compound is only 3-fold less potent than the ring open analogue and cannot adopt the closed binding conformation, but less selective. The X-ray structure (Fig. 2e) showed that the pyrrolidine amide binds analogously to **24** in the open conformation, making a hydrogen bond with Asn859 but not Lys745, in this case in a low energy small molecule conformation. Compound **27** also retained good in vitro stability in human liver microsomes and hepatocytes. As **24** suffered from chemical stability issues (hydrolysis of the amide to acid under acidic conditions, hypothesized to proceed via a cyclic intermediate formed through reaction on the pyrimidine) alkene-linked and methyl sulfone analogues were prepared. The alkenyl analogue **28** shows reduced potency, potentially due to disruption of the ideal bound conformation- the intramolecular hydrogen bond is lost and allylic strain will favor positioning of the amide in the conformation shown in the table. Consistent with the removal of metabolic soft spots and low LogD, **28** shows good in vitro metabolic stability. The sulfone analogue **29** and ether-linked variant **30** both show reasonable potency, good in vitro metabolic stability and low LogD. X-ray structures of the two compounds are shown in Figures 2f and 2g. In both cases one of the sulfone oxygen atoms is able to make a hydrogen bond with Lys745 although the conformation of the linkers is quite different, reflecting the difference in lowest energy ligand conformation. Interestingly, while having equivalent TMLR potency, sulfones **29** and **30** are also in a different position than in the piperidine sulfone analogue **17** (Figure 2h).

Although none of the structurally-diverse methoxy piperidine replacements shown above increased potency, the methoxy piperidine metabolic soft spot was successfully removed with

retention of potency and selectivity over wtEGFR. When tested against a panel of 220 kinases at 1  $\mu$ M compounds **17**, **29**, and **30** retained selectivity compared with **2** whilst **27** was considerably more promiscuous (see Supporting Info Table S1 page S2). The reduced TMLR/wt and kinase selectivity of **27** could possibly be due to the change in interactions within the binding site.

**Table 6.** In vitro and in vivo rat clearance for a selection of analogues.

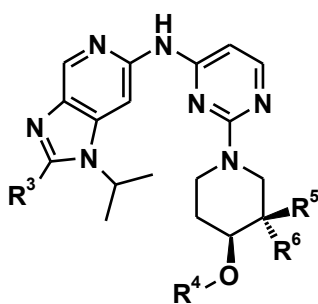
compd	RLM <sup>a</sup> Cl <sub>hep</sub> (mL/min/kg)	RH <sup>b</sup> Cl <sub>hep</sub> (mL/min/kg)	IV dose (mg/kg)	Rat Cl <sub>p</sub> <sup>c</sup> (Cl <sub>u</sub> ) <sup>d</sup> (mL/min/kg)	Calc. pKa <sup>e</sup>
<b>17</b>	26	24	0.5	165 (934)	3.6
<b>24</b>	16	10	0.5	250 (909)	3.5
<b>29</b>	22	21	1.0	158 (707)	3.4
<b>30</b>	19	9	0.5	53 (156)	0.8
<b>31</b>	10	9	0.5	50 (200)	1.3

<sup>a</sup> RLM: Rat liver microsomes; <sup>b</sup> RH: rat hepatocytes; <sup>c</sup> Cl<sub>p</sub>: plasma clearance; <sup>d</sup> Cl<sub>u</sub>: unbound plasma clearance (Cl<sub>u</sub>= Cl<sub>p</sub>/F<sub>u</sub> where F<sub>u</sub> is the fraction unbound in plasma); <sup>e</sup> Calculated using ACD Percepta ® (GALAS) using a 2-substituted pyrimidine sub-structure. See experimental section for details of assay errors and controls.

However, in vivo rat PK of five diverse analogues with improved microsomal and hepatocyte stability showed high clearance for those which retained TMLR potency (Table 6), with total clearance in excess of liver blood flow for **17**, **24** and **29**. Chemical instability due to amide hydrolysis was noted for **24** but the apparent extra-hepatic clearance of **17** and **29** is not so easily explained. Both total and unbound plasma clearance were lower for analogues **30** and **31** which have reduced TMLR potency. It was noted that **30** and **31** have significantly lower calculated pKa of the pyrimidine nitrogen indicative of reduced electron density. The empirical observation that increased in vivo metabolic stability correlates with reduced electron density on the pyrimidine seems logical as the reduced electron density of the heterocycle could slow ring

oxidation as well as glucuronidation of the hinge-binding NH. This trend was shown to some extent in the hepatocyte stability data where **30** and **31** are more stable than **17** and **29**. Based on these findings, principally the in vivo data, fluoro piperidine analogues were conceived in order to retain the potency of the methoxy or hydroxyl piperidine but reduce electron density on the pyrimidine in order to improve metabolic stability.<sup>57</sup> It has been proposed that equatorial 3-fluoro and 3,3-difluoro substitutions have the greatest effect on piperidine pKa,<sup>58</sup> and thus, presumably, pyrimidine electron density in the case of our TMLR inhibitors.

**Table 7.** In vitro potency and physicochemical properties of fluoropiperidine analogues. All analogues are racemic, relative stereochemistry shown.



compd	R3	R4	R5	R6	TMLR Ki <sub>app</sub> (nM)	wtEGFR Ki <sub>app</sub> (nM)	LogD	LLE <sup>a</sup>	H1975 EGFR IC <sub>50</sub> (Prolif.) (μM)	p- EGFR IC <sub>50</sub> (Prolif.) (μM)	H292 p-EGFR IC <sub>50</sub> (Prolif.) (μM)	Rat Cl <sub>p</sub> <sup>b</sup> (Cl <sub>u</sub> ) <sup>c</sup> (mL/min/kg)
<b>2</b>	Me	Me	H	H	20	1200	2.3	5.4	0.88 (7.0)	--		
<b>32</b>	CH <sub>2</sub> OH	Me	H	H	19	400	2.3	5.4	2.36 (6.5)	--		
<b>33</b>	Me	Me	F	H	2.7	1080	2.3	6.3	0.25 (0.56)	>10		
<b>34</b>	CH <sub>2</sub> OH	Me	F	H	4.3	150	2.1	6.3	0.29 (0.88)	>10		107 (584)
<b>35</b>	Me	H	F	H	13	910	1.5	6.3	1.0 (1.6)	--		90 (545)
<b>36</b>	CH <sub>2</sub> OH	H	F	H	16	>0.53	1.6	6.2	2.53 (>10)	>10		151 (382)
<b>37</b>	CH <sub>2</sub> OH	Me	F	F	7.4	249	2.8	5.3	1.0 (2.38)	>10		

<b>38</b>	Me	H	F	F	9.5	>403	2.6	5.4	1.04 (1.7)	>10
<b>39</b>	Me	Me	H	F	44	1840	2.5	4.8	--	--
<b>40</b>	CH <sub>2</sub> OH	Me	H	F	57	540	2.1	5.1	--	--

<sup>a</sup>LLE calculated using measured LogD; <sup>b</sup> Cl<sub>p</sub>: plasma clearance; <sup>c</sup> Cl<sub>u</sub>: unbound plasma clearance (Cl<sub>u</sub>= Cl<sub>p</sub>/F<sub>u</sub> where F<sub>u</sub> is the fraction unbound in plasma). See experimental section for details of assay errors and controls.

On profiling the fluoro piperidine analogues (data shown in Table 7) it was immediately clear that, aside from any potential impact on PK, both 3,3-di-fluoro (**37** and **38**) and cis mono-fluoro (**33-36**) substitution provided a significant increase in potency against TMLR but not wtEGFR in the biochemical, p-EGFR auto-phosphorylation and cell proliferation assays. Profiling against panel of 220 kinases at 1 μM confirmed that cis-fluoro substitution only increased potency against TMLR with no change in the inhibition of other kinases compared to the des-fluoro analogue: compound **33** inhibited 25 kinases 40-80% and 10 kinases >80% with the same pattern of inhibition as **2** (see Supporting Information page S2). Conversely, trans mono-fluoro (**39** and **40**) substitution reduced potency. Synthesis of unsubstituted and 3-fluoropiperidine analogues showed that fluorine substitution alone had no effect on potency (data not shown) further demonstrating the synergy of the cis OMe/OH and F substituents. Further analysis revealed that the cis-mono fluoro substitution increased potency without an increase in measured LogD whereas the increase in potency of the di-fluoro analogues was almost certainly lipophilicity-driven. This is illustrated in a plot of pKi vs LogD (Figure 3) where both pairs of cis-mono fluoro piperidine analogues are differentiated.

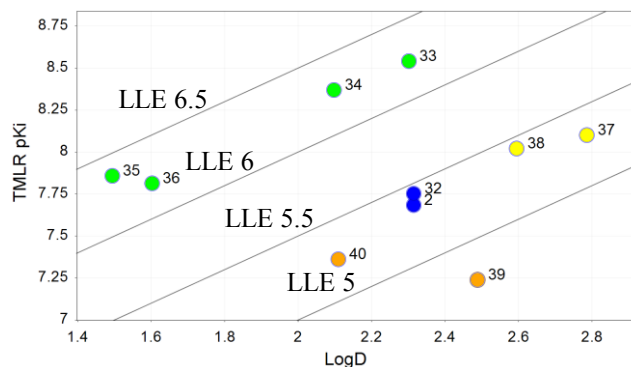


**Figure 3.** TMLR pKi vs measured LogD for hydroxyl and methoxy fluoro piperidine analogues. Lines of equal LLE, calculated using measured LogD, shown. Points annotated with compound numbers. Increased LLE is only seen for cis-monofluoro analogues. Green: cis-monofluoro; blue: des-fluoro; yellow: gem-difluoro; orange: trans-monofluoro.

An X-ray structure obtained from soaking diastereomeric mixture **33** with TMLR preferentially yielded crystals of the 3R-4S enantiomer (Figure 4). In this structure the fluorine was in an axial conformation and within a short distance of the methionine gatekeeper as well as Lys745, possibly positively interacting with either or both of these residues due to the ability of fluorine to form polar, hydrophobic or multipolar interactions.<sup>59</sup> It has been shown that this amphiphilic character can be correlated to the <sup>19</sup>F NMR chemical shift due to the influence of the local environment of fluorine on the character of the C-F bond.<sup>60</sup> <sup>19</sup>F NMR shows a large dispersion, >300 ppm, depending on the number of oxygen, sulfur, nitrogen and other halogen atoms in the  $\alpha$ ,  $\beta$ , and  $\gamma$  positions. High shielding (shift > -160 ppm) has been shown to strongly correlate with proximity to NH side-chains in PDB structures.<sup>60</sup> The hydrogen bond formed by fluorine may well be very weak<sup>61</sup> but it has been postulated that CHF is a better hydrogen bonding group than CF<sub>2</sub>.<sup>62</sup> <sup>19</sup>F NMR for the piperidinyl pyrimidines (see Supporting Info page S91) showed that for the hydroxyl piperidines the cis-fluorine is more shielded (electron rich) than the trans-fluorine (<sup>19</sup>F  $\delta$  -200 and -188 ppm respectively). It has been discovered that when

1  
2  
3 within 3 Å of an oxygen atom in a low energy conformation, fluorine substitution for hydrogen  
4  
5 can lead to a lowering, or no increase, in LogD despite the addition of a lipophilic atom.<sup>63</sup>  
6  
7  
8 Indeed it is the case that there is no significant change in LogD between direct pairs **2** and **33**, **32**  
9  
10 and **34**. The increased shielding observed in the <sup>19</sup>F NMR of the cis-fluoro piperidine is also  
11  
12 possible confirmation of the O-F “interaction”. Although this effect is not fully understood it has  
13  
14 been proposed that fluorine-induced polarization of the proximal oxygen atom could lead to  
15  
16 stronger H-bonds involving this atom.<sup>64</sup> In cis-fluoro hydroxy and methoxy piperidines on our  
17  
18 scaffold this polarization would increase the hydrogen bond acceptor ability of the  
19  
20 ether/hydroxyl oxygen, strengthening the energy of interaction with Lys745. In trans-fluoro  
21  
22 hydroxyl and methoxy piperidines the F...O distance is also <3 Å but the fluorine is positioned  
23  
24 equatorially and unable to make optimal lipophilic contacts. Fluorine substitution can also affect  
25  
26 piperidine conformation. When positioned on a piperidine ring fluorine prefers to be in the axial  
27  
28 conformation,<sup>65</sup> but this conformational preference has only been studied in the case of  
29  
30 protonated piperidines where there can be an H-F hydrogen bond. For un-protonated piperidines  
31  
32 steric factors (A 1,3-strain) would still favor the equatorial conformation, albeit marginally. An  
33  
34 additional conformational factor is the gauche effect- the orbital interaction between the σ C–H  
35  
36 bond and the σ\* C–F bond, hyperconjugation- which is maximized when the C-H and C-F bonds  
37  
38 are anti-periplanar. Further discussion of the influence of fluoro substitution is presented below.  
39  
40  
41  
42  
43  
44  
45  
46  
47  
48  
49  
50  
51  
52  
53  
54  
55  
56  
57  
58  
59  
60

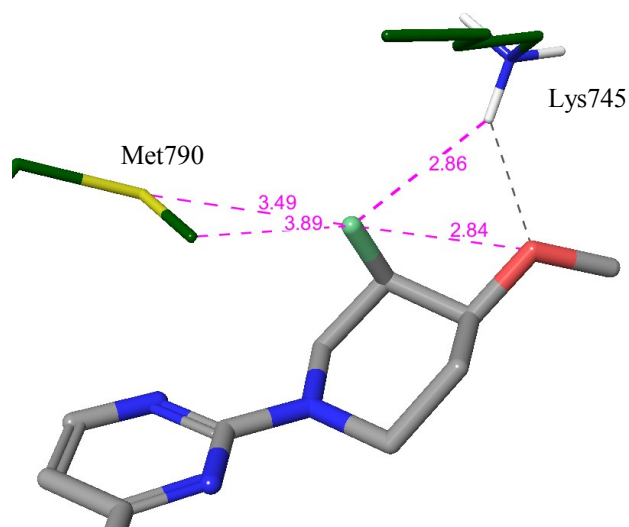


**Figure 4.** Representation of the X-ray structure of **33** (PDB code 5CAQ) showing the interactions of the fluoro methoxy piperidine with key residues Met790 and Lys745. Inter-atom distances indicated by dashed purple lines with values in Å. The fluorine is positioned axially and within 3.5 Å of Met790 and 2.9 Å of the NH of Lys745. The F-O distance is 2.8 Å. **33** was soaked as mixture of enantiomers, the 3R, 4S enantiomer crystallizing preferentially.

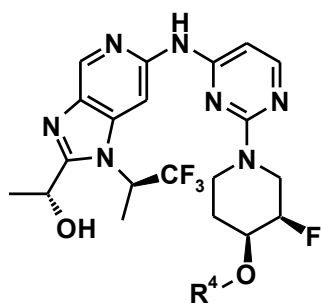
Compared to the des-fluoro analogue **15**, no change of rat in vivo clearance was seen with the cis-fluoro hydroxy or fluoro methoxy analogues (**34**: 1 mg/kg IV Cl<sub>p</sub> (Cl<sub>u</sub>) 107 (584) mL/min/kg; **35**: 5 mg/kg IV Cl (Cl<sub>u</sub>) 90 (545) mL/min/kg; **36**: 0.5 mg/kg IV Cl<sub>p</sub> (Cl<sub>u</sub>) 151 (382) mL/min/kg). Even if the hypothesis of the correlation of lower pyrimidine pK<sub>a</sub> and electron density were true, the fluorines in **34**, **35** and **36** are axial and so may have a negligible electron withdrawing effect (see above). In the absence of data for compounds in Table 7 it would be assumed that metabolism of **34** is driven by de-methylation, and **35-36** driven by Phase II conjugation, and perhaps this is the case, but in vitro stability data for **34**, **35** and **36** still under-predicted in vivo clearance.<sup>66</sup> The trans analogues, where the fluorine would be equatorial, were not profiled and

1  
2  
3 for difluoro compounds the increase in lipophilicity would probably counteract any benefit from  
4  
5 reduced electron density.  
6  
7

8  
9 Due to the TMLR-specific increase in potency without added lipophilicity, the methoxy and  
10 hydroxyl cis mono-fluoro piperidine substituents were combined with small changes to the  
11 azabenzimidazole 1- and 2- substituents focusing on modifications which would block  
12 metabolism of the 2-methyl group and increase lipophilic interactions in the ribose pocket  
13 without introducing further metabolic soft spots. Thus, combinations were made with the  
14 trifluor-isopropyl group (as in **14**) together with methyl, hydroxymethyl and 2-hydroxyethyl  
15 groups at the azabenzimidazole 2-position. The rationale for making these changes was that the  
16 hydroxymethyl 2-substituent was the active metabolite of the 2-methyl compounds and steric  
17 bulk was added both to block oxidation and glucuronidation of the hydroxyl compounds.  
18 Additionally, the change to trifluor-isopropyl in **14** is LLE neutral- potency and LogD are  
19 increased to the same extent. The most potent combination analogues prepared, **41** and **42**  
20 (profiled initially as mixtures of diastereomers, cis OH/F and OMe/F) are shown in Table 8. All  
21 possible stereoisomers of **41** and **42** were prepared but none was more potent (data not shown).  
22 Compared to earlier direct analogues (**42** with **36**; **41** with **34**) a ~10-fold increase in cellular  
23 potency and 3.5 to 6.5 -fold increase in affinity is apparent, improvements which come without  
24 any significant increase in measured LogD (~0.2 units), whereas cLogP is increased ~0.6 units.  
25 The increase in potency against TMLR was shown to be accompanied by retention of kinase  
26 selectivity: when profiled against a panel of 308 kinases at 1  $\mu$ M compounds **42a** and **42b** (the  
27 individual diastereomers of **42**) showed >80% inhibition of only 14 individual kinases (see  
28 Supporting Information table S2 page S3). The analogues **41** and **42** were also tested against the  
29 isolated TMdel enzyme and in a TMdel expressing cell line: erlotinib-resistant PC9 cells (PC9  
30  
31  
32  
33  
34  
35  
36  
37  
38  
39  
40  
41  
42  
43  
44  
45  
46  
47  
48  
49  
50  
51  
52  
53  
54  
55  
56  
57  
58  
59  
60

(ER)). These cells are grown in the presence of a high concentration of erlotinib in order to cause and maintain the T790M resistance mutation. Potency in the biochemical assay against the TMdel enzyme is significantly weaker than TMLR, a trend which was not evident in earlier analogues.<sup>39</sup> However, cell potency, which is obviously more important, is actually better against PC9(ER) than H1975. Increased proliferation potency in the PC9(ER) cells could be due to greater sensitivity to inhibition of the EGFR pathway, but this should not affect pEGFR EC<sub>50</sub>. The low cell drop-off from TMdel Ki to PC9(ER) pEGFR EC<sub>50</sub>, given the low K<sub>M</sub>[ATP] of this enzyme, is curious and is perhaps related to the protein construct used in the biochemical assay.

**Table 8.** Profiles of fluoro-hydroxy and fluoro-methoxy combination analogues.



(Piperidine stereochemistry relative, other stereochemistry absolute)

	41 (R <sup>4</sup> = Me)	42 (R <sup>4</sup> = H)
TMLR Ki <sub>app</sub> (nM)	1.1	2.5
TMdel Ki <sub>app</sub> (nM)	7.0	6.0
wt EGFR Ki <sub>app</sub> (nM)	122	313
LogD	2.2	1.8
pEGFR H1975 IC <sub>50</sub> (nM)	21	261
H1975 prolif. EC <sub>50</sub> (nM)	112	900
pEGFR PC9(ER) IC <sub>50</sub> (nM)	27	81
PC9(ER) prolif. EC <sub>50</sub> (nM)	90	170
pEGFR H292 IC <sub>50</sub> (nM)	>10,000	>10,000

H292 proliferative EC <sub>50</sub> (nM)	7,800	>10,000
Microsomal Cl <sub>hep</sub> h/r/m/d/c <sup>a</sup> (mL/min/kg)	15/28/81/24/36	7/11/73/18/19
Hepatocyte Cl <sub>hep</sub> h/r/m/d/c <sup>a</sup> (mL/min/kg)	10/25/75/10/30	4/13/68/4/19
Rat IV (5 mg/kg) Cl <sub>p</sub> /Cl <sub>u</sub> <sup>b</sup> (mL/min/kg)	23 (334)	71 (348)
T ½ (h), V <sub>ss</sub> (L/kg)	1.7, 3.7	0.71, 3.5
Rat %F	85 <sup>c</sup>	29 <sup>d</sup>

<sup>a</sup> m: mouse; r: rat, d: dog, c: cynomolgus monkey h: human; <sup>b</sup> Cl<sub>p</sub>: plasma clearance, Cl<sub>u</sub>: unbound plasma clearance (Cl<sub>p</sub>/F<sub>u</sub> where F<sub>u</sub> is the fraction unbound in plasma); <sup>c</sup> formulated in 10% DMSO/10% Cremophor EL in saline; <sup>d</sup> formulated in 10% ethanol/60% PEG100/30% SQ water. See experimental section for details of assay errors and controls.

Compared with published covalent and noncovalent TMLR inhibitors, compounds **41** and **42** show substantially increased selectivity in cell p-EGFR and proliferation assays (see Supporting Information Table S5 page S11). Compound **41** is more potent than AP26113, AZD9291 and WZ4002 in the p-EGFR assay, but ~10-fold less potent than the covalent analogues in proliferation assays reflecting the different mechanism of action.

The individual diastereoisomers making up **41** were prepared and profiled and found to have essentially identical in vitro potency (see Supporting Information Table S4 page S11). X-ray structures with TMLR showed that the fluorine of **41a** (3R, 4S) is in the same position as with earlier analogue **33** but in the diastereoisomer **41b** (3S, 4R) (Figure 5a and 5b) the position is transposed. Here the fluorine is still within close proximity of the piperidine ether oxygen but not the catalytic lysine or the sulfur of Met790. Instead, the fluorine is within 3.3 Å of Val726 and 3.6 Å of the carbon atom of the methyl of Met790, possibly making lipophilic contacts with these residues. These structures also revealed the interactions of the azabenzimidazole 1- and 2-substituents. The hydroxyl group at the azabenzimidazole 2-position is able to make a water-

1  
2  
3 mediated interaction with Asp800 and the backbone NH of Cys797. One of the fluorines of the  
4  
5 trifluoromethyl has the appropriate vector and distance relative to the base of the carbonyl of  
6  
7 Leu718 to make a positive interaction<sup>67</sup> and the trifluoromethyl group itself fills the lipophilic  
8  
9 ribose pocket. Additionally, the trifluoromethyl is within contact distance (3.2 Å) of the  
10  
11 piperidine, potentially making the bound conformation of the molecule more favorable. A  
12  
13 structure of **41a** in wtEGFR was also obtained (Figure 6). Despite the >100-fold lower potency  
14  
15 against the wt enzyme, the binding mode and position of all residues (except the gatekeeper) is  
16  
17 essentially identical indicating that the potency difference arises from the difference in  
18  
19 interactions with the gatekeeper residues.  
20  
21  
22  
23

24 For the diastereomeric mixture **42** <sup>19</sup>F NMR shifts of -72 ppm (CF<sub>3</sub>) and -198 ppm (CHF) are  
25  
26 seen consistent with a de-shielded CF<sub>3</sub> fluorine environment and a shielded piperidine CHF,  
27  
28 correlated in the literature with hydrophobic/multipolar and polar interactions respectively.  
29  
30 However, the hypothesis that the observed potency increase is due to hydrogen bonding of the  
31  
32 fluorine does not fit well with the rest of the data. The X-ray data, the equivalent potency of the  
33  
34 two diastereomeric pairs **41a/41b** and **42a/42b** (vide infra) and the *specific* increase in TMLR  
35  
36 potency over wtEGFR suggests that fluoro substitution increases potency by enhancing the  
37  
38 hydrogen-bonding capability of the ether oxygen and, more importantly, making lipophilic  
39  
40 contacts with the methionine gatekeeper and other neighboring lipophilic residues.  
41  
42  
43  
44  
45  
46  
47  
48  
49  
50  
51  
52  
53  
54  
55  
56  
57  
58  
59  
60

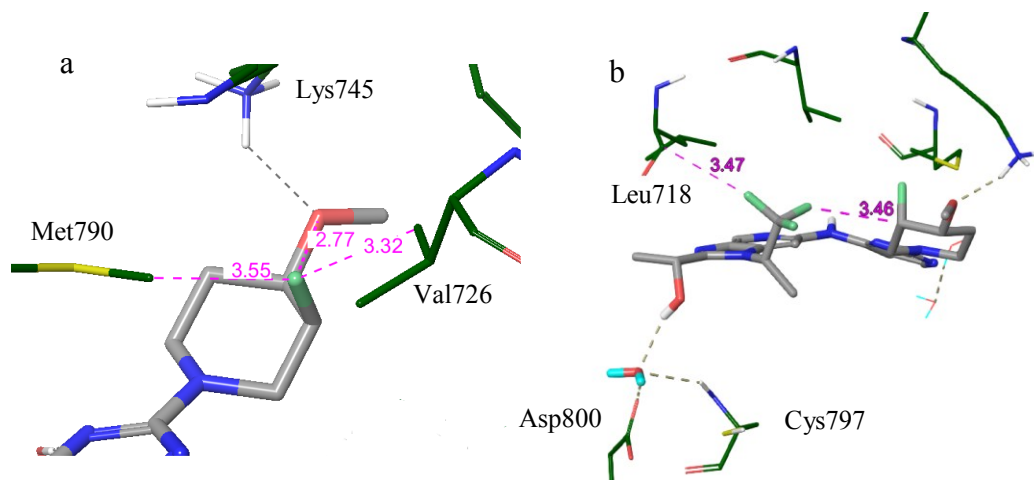


**Figure 5.** Representations of X-ray structure of **41b** in complex with TMLR (PDB accession code 5CAU). Inter-atom distances shown by purple dashed lines, values in Å; hydrogen bonds shown by gray dashed lines, some residues removed for clarity. a) Interactions of the 3S, 4R piperidine with neighboring residues Met790, Lys745 and Val726; b) image showing the multipolar interaction of the CF<sub>3</sub> group with the base of the carbonyl of Leu718 and the close distance (3.5 Å) with the piperidine ring.

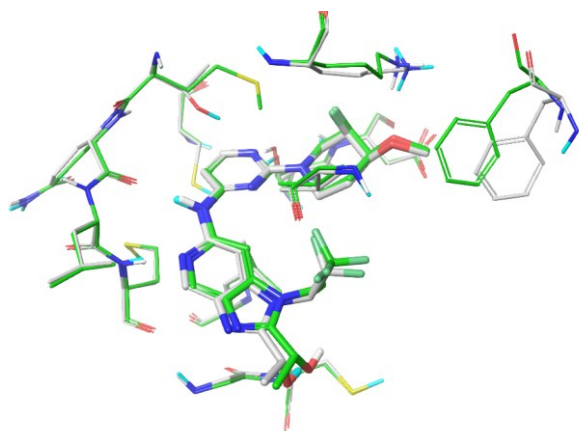


**Figure 6.** Representation of the X-ray structure of **41a** in TMLR and wtEGFR (PDB codes 5CAV and 5CAS). The TMLR structure and ligand are shown in green, wtEGFR and ligand in light gray.

1  
2  
3 The in vitro metabolic stability in rat liver microsomes and hepatocytes of the hydroxyl  
4 analogue **42** was superior to the methoxy analogue **41** but in vivo both compounds have  
5 moderate to high clearance and near identical unbound clearance, with **42** appearing as the major  
6 identified metabolite of **41** (see Table 8). Despite lower potency, the hydroxyl analogue **42** was  
7 progressed preferentially due to higher human hepatocyte stability, increased solubility and the  
8 removal of complication of an active metabolite with the methoxy analogue (i.e. **41**). Since the  
9 in vitro liver microsome metabolic stability data is in line with in vivo clearance observed in dog  
10 and cynomolgus monkey, (see Supporting Information page S10), low to moderate clearance of  
11 **42** in human was predicted based on IVIVC. Similar results were obtained using allometric  
12 scaling.<sup>68</sup> Due to the identical profiles of individual isomers (see Supporting Information pages  
13 S5 and S10) the 1:1 diastereomeric mixture **42** was profiled in vivo using the H1975 xenograft  
14 model.

15  
16  
17  
18  
19  
20  
21  
22  
23  
24  
25  
26  
27  
28  
29  
30  
31  
32 Oral administration of 300 mg/kg daily for 3 days was sufficient to suppress EGFR  
33 phosphorylation (>90% inhibition)<sup>69</sup> as well as phosphorylation of the downstream targets ERK  
34 (>90% inhibition) and AKT (>65% inhibition) for 8 hours (Fig. 7). The in vivo EC<sub>50</sub> for  
35 inhibition of pERK and pAKT was estimated at ~0.3 μM and ~0.5 μM free respectively which is  
36 in line with in vitro data. Due to supra-proportional exposure between 100 and 300 mg/kg, when  
37 **42** was administered at 100 mg/kg daily much weaker pathway suppression was evident.  
38 Nevertheless potent inhibition of receptor phosphorylation, ERK and AKT was achieved at early  
39 time points (Fig 7).  
40  
41  
42  
43  
44  
45  
46  
47  
48  
49  
50  
51  
52  
53  
54  
55  
56  
57  
58  
59  
60

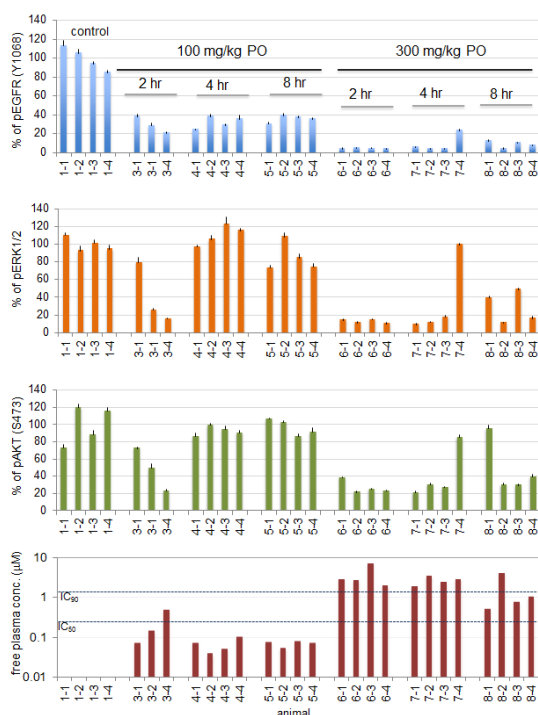


**Figure 7.** Compound **42** was administered orally (PO) to H1975 tumor-bearing mice once a day for 3 days with either 100 mg/kg or 300 mg/kg respectively. Tumors were collected at indicated times (post last dose) and phosphorylation of EGFR, ERK and AKT was determined using commercially available MSD assays. Lines on the free concentration plot show the in vitro H1975 p-EGFR IC<sub>50</sub> and IC<sub>90</sub>. Error bars represent mean ± SD. Plasma concentrations of **42** were measured using a liquid chromatography-tandem mass spectrometry assay and free concentration was calculated using Fu of 0.207.

These data demonstrate that a noncovalent reversible T790M double-mutant selective compound has the potential to provide a substantial benefit to patients harboring erlotinib or gefitinib resistant tumors. However, given the clinical efficacy without wtEGFR inhibition associated side-effects seen with 3<sup>rd</sup> generation covalent compounds the clinical use of highly-selective, reversible T790M double mutant EGFR inhibitors should be supported by further preclinical evidence. For example: demonstration that increased wt/TMLR selectivity window

1  
2  
3 translates into improved therapeutic index, examination of resistance mechanisms and potency  
4  
5 against tumors expressing the C797S mutation.  
6  
7

## 8 9 10 **CONCLUSION**

11  
12  
13  
14 We have shown how a strategy focusing on the optimization of potency in the context of  
15 measured LogD whilst mitigating metabolic stability issues identified in vitro and in vivo has  
16 been applied to the optimization of a reversible, T790M selective, lead compound. This focused  
17 optimization strategy helped avoid pitfalls of low solubility and reduced selectivity often  
18 encountered in lead optimization. The progress from optimization of the first HTS hit to early  
19 lead **1** (described in our previous paper) to breakthrough compound **33** to optimized compound  
20 **42** can be traced through consistent increases in LLE (HTS hit: 2.6; **33**: 6.3; **42**: 7.1).  
21  
22  
23  
24  
25  
26  
27  
28  
29

30  
31 The key transformation- cis-fluoro substitution on the 4-hydroxy and methoxy piperidine- led  
32 to a surprisingly specific increase in TMLR biochemical and cellular potency without any  
33 increase in LogD. The reasons for this increase in potency are probably multifactorial but the  
34 data are most consistent the axial fluorine interacting with the methionine gatekeeper and other  
35 neighboring residues. Further optimization through modification of the azabenzimidazole  
36 substituent led to compounds with low nM enzyme potency, again with minimal LogD increase,  
37 >100-fold selectivity for the T790M mutants and cell potency in the low  $\mu\text{M}$  range. Following  
38 this, a diastereomeric pair of compounds showed oral single agent activity in vivo suppressing  
39 the EGFR pathway >90% in a TMLR-driven H1975 xenograft model.  
40  
41  
42  
43  
44  
45  
46  
47  
48  
49  
50

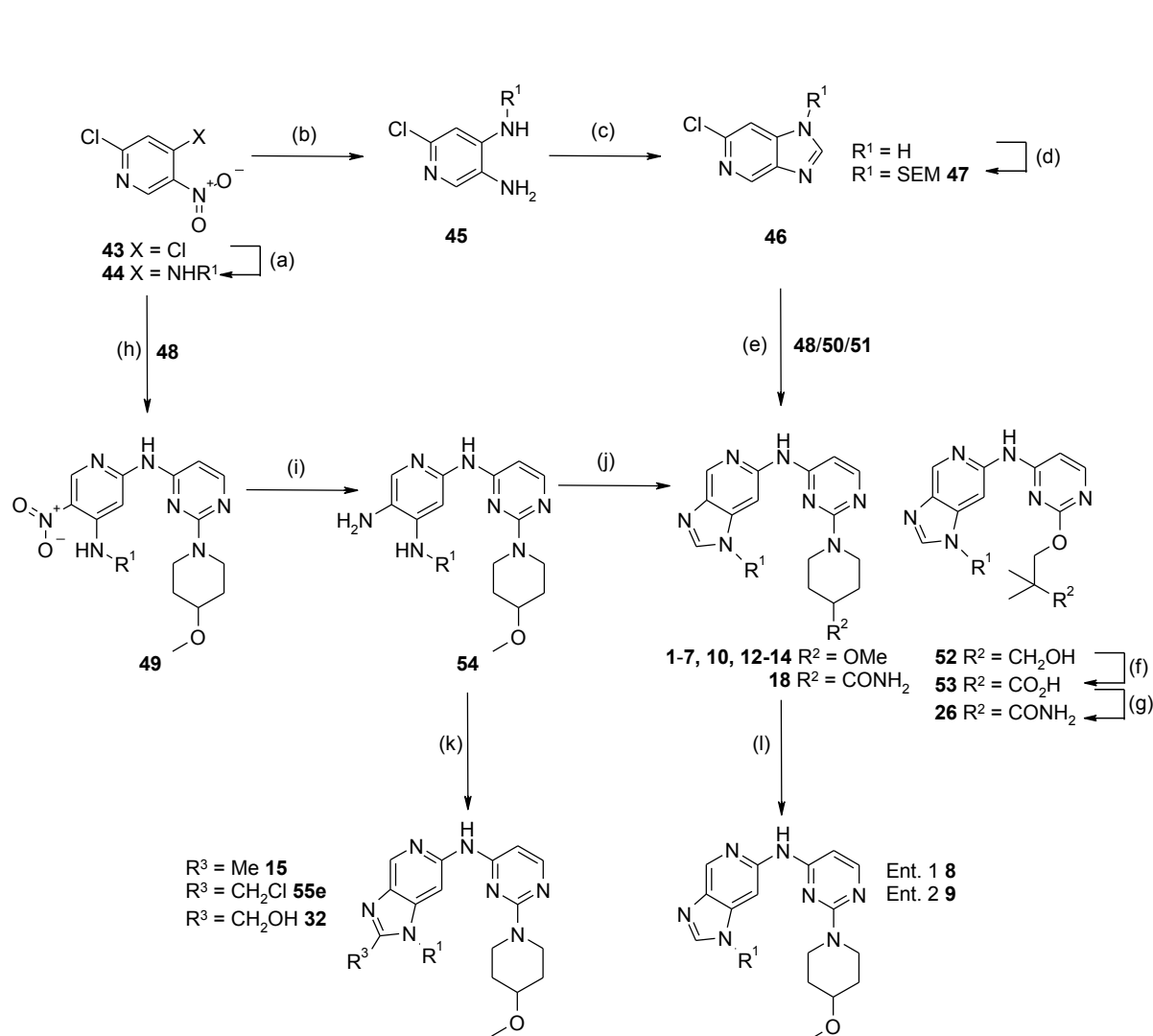
51  
52 As well as demonstrating the potential future utility of reversible noncovalent T790M-selective  
53 inhibitors in treating erlotinib and gefitinib resistant cancer patients, this work highlights a  
54 number of aspects of medicinal chemistry doctrine: the structural similarity of leads and  
55  
56  
57  
58  
59  
60

1  
2  
3 optimized compounds, the utility of fluorine in the optimization of small molecule drugs, and the  
4  
5 judicious application of compound quality metrics as an aid to interpretation of SAR.  
6  
7

## 8 9 10 **SYNTHESIS**

11  
12  
13  
14 The preparation of *N*-substituted aza-benzimidazole analogues **1-10**, **12-15**, **18**, **26** and **32**  
15  
16 was carried out as outlined in Scheme 1. Regiospecific S<sub>N</sub>Ar, followed by reduction and  
17  
18 cyclisation with trimethyl orthoformate, afforded azabenzimidazole template **46**. A final  
19  
20 Buchwald-Hartwig coupling furnished targets **1-4**, **6-7**, **10**, **12-14** and **18**. Chiral resolution of  
21  
22 racemate **7** afforded **ent-8** and **ent-9**. For example **5**, Table 1, the RHS unit was installed on  
23  
24 intermediate **44** via Buchwald-Hartwig coupling, followed by reduction and subsequent  
25  
26 cyclisation to generate the final target (sequence **49-54-5**). Variation of R<sup>3</sup> was facilitated by  
27  
28 condensation of **54** with the appropriate orthoester derivative (**15** and **32**).  
29  
30  
31  
32

33  
34  
35 Scheme 1: Synthetic route for azabenzimidazole *N*-substituent analogues **1-10**, **12-15**, **18**, **26** and  
36  
37 **32**. R groups as defined in Tables 1, 2, 3, 5 and 7 unless stated.<sup>a</sup>  
38  
39  
40  
41  
42  
43  
44  
45  
46  
47  
48  
49  
50  
51  
52  
53  
54  
55  
56  
57  
58  
59  
60

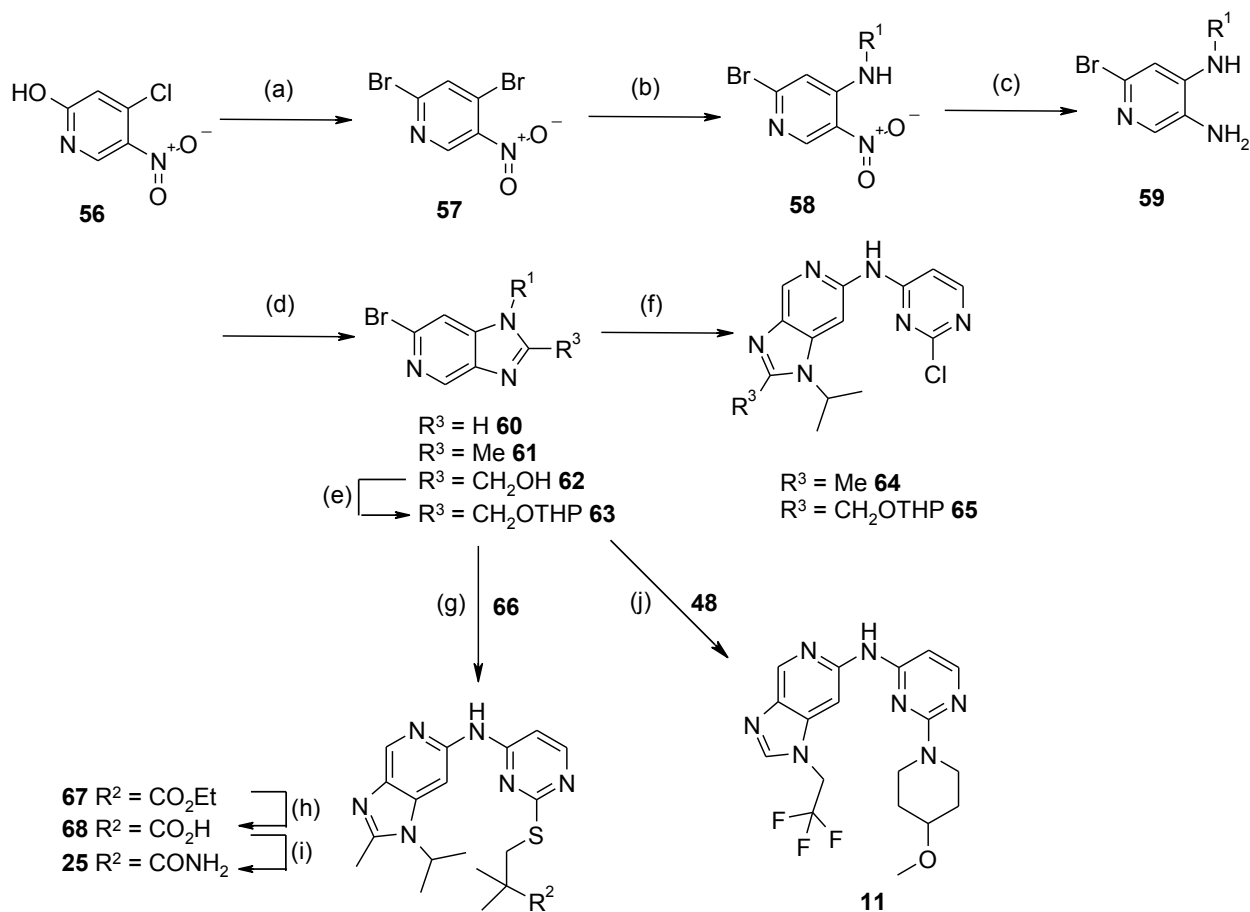


37  
38  
39  
40  
41  
42  
43  
44  
45  
46  
47  
48  
49  
50  
51  
52  
53  
54  
55  
56  
57  
58  
59  
60

<sup>a</sup>(a) **43**, R<sup>1</sup>NH<sub>2</sub>, THF, rt, 2 h (62%-quant.); (b) **44**, Fe, NH<sub>4</sub>Cl, EtOH/H<sub>2</sub>O, 78 °C, 20 h (70%-quant.); (c) (MeO)<sub>3</sub>CH, HCO<sub>2</sub>H, 80-120 °C, 18 h (50-92%); (d) For R<sup>1</sup> = H, NaH, DMF, SEMCl, 0 °C to rt, 1 h (60%); (e) (i) For **1**, **3-4**, **6-7**, **10**, **12-14**, 2-(4-methoxypiperidin-1-yl)pyrimidin-4-ylamine **48**, XPhos, Pd<sub>2</sub>(dba)<sub>3</sub>, Cs<sub>2</sub>CO<sub>3</sub>, 1,4-dioxane, 120 °C, 12 h (12-78%); (ii) For **18** - 1-(4-aminopyrimidin-2-yl)piperidine-4-carboxylic acid amide **50**, XPhos, Pd<sub>2</sub>(dba)<sub>3</sub>, Cs<sub>2</sub>CO<sub>3</sub>, 1,4-dioxane, 120 °C, 12 h (8%); (iii) For **2**, 2-(4-methoxypiperidin-1-yl)pyrimidin-4-ylamine **48**, chloro{[BrettPhos][2-(2-aminoethylphenyl)palladium(II)]}/[BrettPhos], NaO<sup>t</sup>Bu, <sup>t</sup>BuOH, 120 °C, 2 h (6%); (iv) For **26** - 2,2-dimethylpropane-1,3-diol **51**, XantPhos Pd<sub>2</sub>(dba)<sub>3</sub>.CHCl<sub>3</sub>, Cs<sub>2</sub>CO<sub>3</sub>, 1,4-dioxane, 100 °C, 1 h (55%); (f) **52**, PDC, DMF, rt, 24 h (19%); (g) **53**, CDI, NH<sub>4</sub>OH, DMF, rt, 18 h (20%); (h) **44e**, 2-(4-methoxypiperidin-1-yl)pyrimidin-4-ylamine **48**, XPhos, Pd<sub>2</sub>(dba)<sub>3</sub>, Cs<sub>2</sub>CO<sub>3</sub>, 1,4-dioxane, 100 °C, 3 h (72%); (i) **49e**, H<sub>2</sub>, Pd/C (10% w/w), EtOAc/MeOH, rt, 18 h (92%); (j) **54e**, (MeO)<sub>3</sub>CH, HCO<sub>2</sub>H, 100 °C, 1 h (27%); (k) (i) For R<sup>3</sup> = Me **15** - **54**: MeC(OEt)<sub>3</sub>, HCO<sub>2</sub>H, μW, 220 °C, 5.5 h (90%); (ii) For R<sup>3</sup> = CH<sub>2</sub>OH **32**: (i) **54**, 2-chloro-1,1,1-trimethoxyethane, p-TSA, 100 °C, 1 h (86%); (ii) **55e**, KOAc, DMF, 100 °C, 45 min (52%); (l) Chiral resolution of **7**, ChiralPak IA column (20 mm x 250 mm), 10% EtOH, 10% TBME and 0.5% DEA in heptane (isocratic), flow rate 18 ml/min (**8**, ent. 1 84%, >99% ee; **9**, ent. 2 78%, 93% ee).

1  
2  
3 In order to fully probe the SAR, and facilitate diversification at the pyrimidine 2-substituent,  
4 late stage intermediates **64/65** were targeted as outlined in Scheme 2. Bromination of **56**,  
5 followed by regiospecific S<sub>N</sub>Ar displacement, reduction and cyclisation with the requisite  
6 orthoester/acid chloride derivative gave **60-62**. A final Buchwald-Hartwig coupling with 2-  
7 chloropyrimidin-4-ylamine afforded key intermediates **64/65**. For **62**, wherein R = CH<sub>2</sub>OH, this  
8 intermediate was further derivatised to the corresponding THP protected analogue **63** prior to  
9 coupling. Direct S<sub>N</sub>Ar displacement of the chloride in **64/65** with appropriately functionalised  
10 primary/secondary amines, primary alcohols or Pd-mediated couplings with the requisite vinyl  
11 boronate were then effected to afford target compounds **16-17**, **19-24**, **27-31** and **33-40** as  
12 outlined in Scheme 3. Alternatively, as revealed in Scheme 2, the intact pyrimidinyl unit could  
13 be installed directly via a Pd-catalysed arylation and this was the strategy adopted for compounds  
14 **11** (Table 1) and **25**.  
15  
16  
17  
18  
19  
20  
21  
22  
23  
24  
25  
26  
27  
28  
29  
30  
31  
32

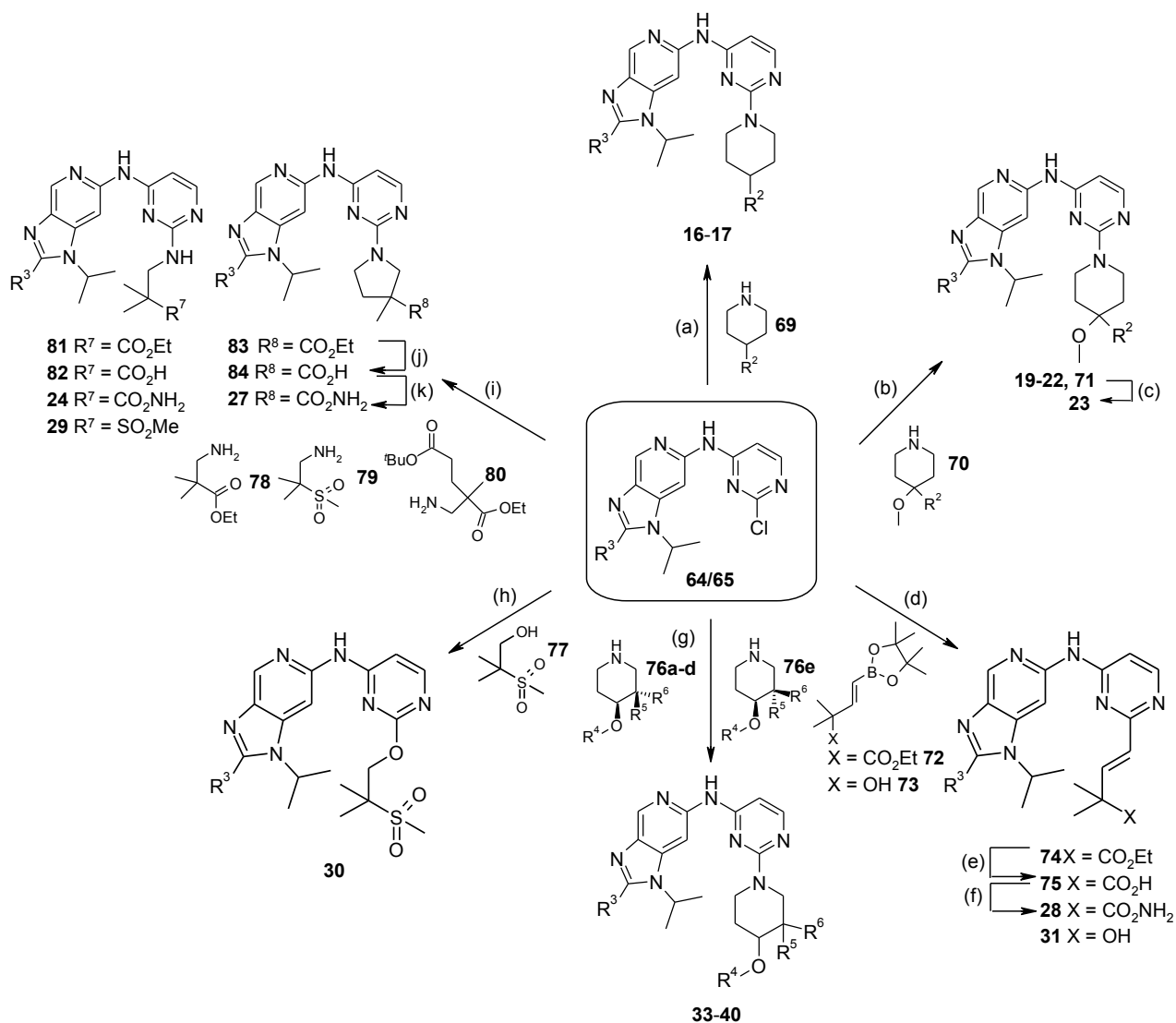
33 Scheme 2: Synthetic route to key intermediate **64/65**, trifluoroethyl derivative **11** and acyclic  
34 analogue **25**. R groups as defined in Tables 1, 2, 3, 5 and 7.<sup>a</sup>  
35  
36  
37  
38  
39  
40  
41  
42  
43  
44  
45  
46  
47  
48  
49  
50  
51  
52  
53  
54  
55  
56  
57  
58  
59  
60



(a) **56**, POBr<sub>3</sub>, CH<sub>3</sub>CN, 80 °C, 2 h (41%); (b) **57**, *i*PrNH<sub>2</sub>, THF, rt, 1 h (quant.); **57**, CF<sub>3</sub>CH<sub>2</sub>NH<sub>2</sub>, THF, rt, 18 h, then 35 °C, 18 h (79%); (c) **59e**, **58**, Fe, EtOH/AcOH, 80 °C, 4 h (R<sup>1</sup> = *i*Pr (94%)); **59h**, **58**, Fe, EtOH/AcOH, rt, 18 h (R<sup>1</sup> = CF<sub>3</sub>CH<sub>2</sub> (94%)); (d) For **60h**, **59h**, (MeO)<sub>3</sub>CH, HCO<sub>2</sub>H, 110 °C, 18 h (54%); For **61e** - (i) **59e**, (EtO)<sub>3</sub>CMe, AcOH, 80 °C, 24 h (88%), (ii) K<sub>2</sub>CO<sub>3</sub>, DMF, 100 °C, 24 h (47%); For **62e** - (i) **59e**, MeCO<sub>2</sub>CH<sub>2</sub>COCl, Et<sub>3</sub>N, DCM, 0 °C, 1 h (67%), (ii) K<sub>2</sub>CO<sub>3</sub>, DMF, 120 °C, 24 h (57%); (e) **62e**, 3,4-dihydro-2H-pyran, p-TSA, THF, 60 °C, 12 h (51%); (f) For **64** - **61e**, 2-chloropyrimidin-4-ylamine, XantPhos, Pd<sub>2</sub>(dba)<sub>3</sub>.CHCl<sub>3</sub>, Cs<sub>2</sub>CO<sub>3</sub>, 1,4-dioxane, 100 °C, 4 h (26%); For **65** - **63e**, 2-chloropyrimidin-4-ylamine, XantPhos, Pd<sub>2</sub>(dba)<sub>3</sub>, Cs<sub>2</sub>CO<sub>3</sub>, 1,4-dioxane, 100 °C, 1 h (91%) (g) **61e**, 3-(4-aminopyrimidin-2-ylsulfanyl)-2,2-dimethylpropionic acid ethyl ester **66**, CuI, *trans*-*N,N'*-dimethylcyclohexane-1,2-diamine, Cs<sub>2</sub>CO<sub>3</sub>, 1,4-dioxane, 90 °C 1.5 h (30%); (h) **67**, LiOH, THF/H<sub>2</sub>O, rt, 4 h then, 50 °C, 20 h then,  $\mu$ W, 100 °C, 4 h (quant.); (i) **68**, NH<sub>4</sub>Cl, HATU, DMAP (cat.), DIPEA, DMF, rt, 3 h (46% over 2 steps); (j) **60h**, 2-(4-methoxypiperidin-1-yl)pyrimidin-4-ylamine **48**, XPhos, Pd<sub>2</sub>(dba)<sub>3</sub>, Cs<sub>2</sub>CO<sub>3</sub>, 120 °C, 18 h (22%).

Scheme 3: Synthetic route to piperidine and related analogues **16-17**, **19-24**, **27-31** and **33-40**.

R groups as defined in Tables 3, 4, 5 and 7. Analogues **33-40** are racemic, relative stereochemistry as defined in Table 3.<sup>a</sup>

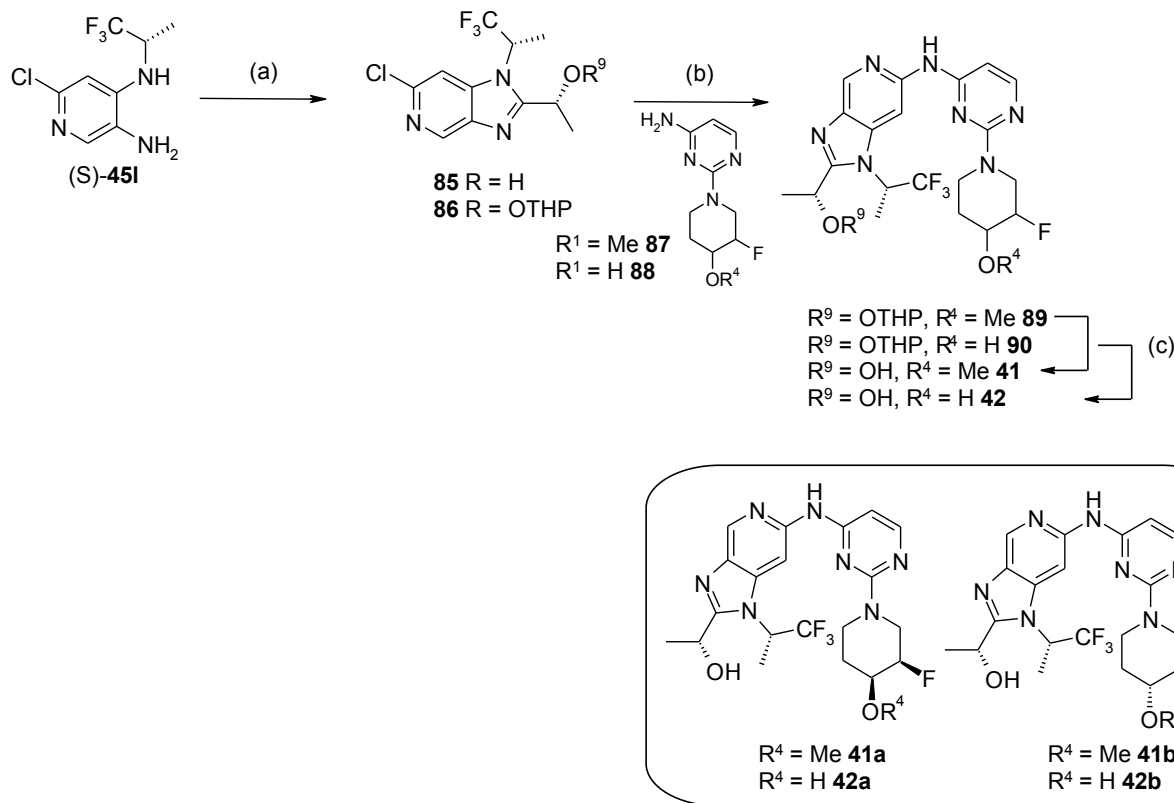


<sup>a</sup>(a) **64**, **69a** (R<sup>1</sup> = OH)/**69b** (R<sup>1</sup> = SO<sub>2</sub>Me), Et<sub>3</sub>N, IPA, μW, 150 °C, 0.5-0.75 h (29-80%); (b) **64**, **70a** (R<sup>1</sup> = CH<sub>2</sub>NMe<sub>2</sub>)/**70b** (R<sup>1</sup> = CH<sub>2</sub>OMe)/**70c** (R<sup>1</sup> = CH<sub>2</sub>OH)/**70d** (R<sup>1</sup> = CH<sub>2</sub>CH<sub>2</sub>OH)/**70e** (R<sup>1</sup> = CH<sub>2</sub>CH<sub>2</sub>N<sub>3</sub>), Et<sub>3</sub>N, IPA, μW, 150 °C, 1 h (14-72%); (c) For **71** to **23**, H<sub>2</sub>, Pd/C, IMS, rt, 16 h (68%); (d) (i) For **74** - **64**, **72**, Pd(dppf)Cl<sub>2</sub>.DCM, 2M Na<sub>2</sub>CO<sub>3</sub>, DME, 100 °C, 16 h (42%); (ii) For **31** - **64**, **73**, Pd(dppf)Cl<sub>2</sub>.DCM, 2M Na<sub>2</sub>CO<sub>3</sub>, DME, 100 °C, 64 h (79%); (e) (i) **74**, LiOH.H<sub>2</sub>O, dioxane, μW, 100 °C, 1 h (quant.); (f) **75**, NH<sub>4</sub>Cl, HATU, DMAP, DIPEA, DMF, rt, 1 h (33%); (g) (i) **76** (**a** R<sup>4</sup> = Me, R<sup>5</sup> = F, R<sup>6</sup> = H; **b** R<sup>4</sup> = H, R<sup>5</sup> = F, R<sup>6</sup> = H; **c** R<sup>4</sup> = Me, R<sup>5</sup> = F, R<sup>6</sup> = F, **d** = R<sup>4</sup> = H, R<sup>5</sup> = F, R<sup>6</sup> = F; **e** = R<sup>4</sup> = Me, R<sup>5</sup> = H, R<sup>6</sup> = F), **64/65**, <sup>i</sup>Pr<sub>2</sub>NEt, IPA, μW, 150

1  
2  
3 °C, 30-60 min. (**33**, **35**, **38**, **39**, 42-70%); (ii) 1.25 M HCl in MeOH, rt, 1 h (**34**, **36**, **37**, **40**, 36-  
4 60% over 2 steps); (h) **64**, **77**, K<sub>2</sub>CO<sub>3</sub>, IPA,  $\mu$ W, 250 °C, 4.5 h (52%); (i) **78** or **79** or **80**, DIPEA,  
5 IPA,  $\mu$ W, 150 °C, 1-10 h (50%-Quant.); For **81** to **24** - (j) **81**, 6M HCl,  $\mu$ W, 120 °C, 1 h (97%);  
6 (k) **82**, NH<sub>4</sub>Cl, HATU, <sup>i</sup>Pr<sub>2</sub>NEt, DMF, rt, 2.5 h (41%); for **83** to **27** - (j) **83**, 3M HCl,  $\mu$ W, 110  
7 °C, 1 h (92% over 2 steps from **64**); (k) **84**, NH<sub>4</sub>Cl, HATU, <sup>i</sup>Pr<sub>2</sub>NEt, DMF, rt, 1.5 h (70%).  
8  
9

10 Fluoropiperidine analogues **41** and **42** were identified and initially profiled as a mixture of  
11 diastereoisomers (cis-rel-OMe/F and OH/F respectively). The azabenzimidazole intermediate **86**  
12 was prepared from (S)-**45I** via cyclisation with the corresponding imidate generated *in situ* from  
13 (R)-lactamide/Meerwein's salt followed by protection of the secondary alcohol. A subsequent  
14 Buchwald-Hartwig coupling with ( $\pm$ )-**87**/ $(\pm)$ -**88**, followed by THP deprotection, afforded cis-rel-  
15 **41** and **42**. The individual diastereoisomers **41a/b** and **42a/b** were in turn prepared by performing  
16 the latter coupling with the appropriate homochiral piperidiny-pyrimidine unit.  
17  
18  
19  
20  
21  
22  
23  
24  
25  
26  
27  
28  
29  
30  
31

32 Scheme 4: Synthetic route to fluoropiperidine analogues<sup>a</sup>  
33  
34  
35  
36  
37  
38  
39  
40  
41  
42  
43  
44  
45  
46  
47  
48  
49  
50  
51  
52  
53  
54  
55  
56  
57  
58  
59  
60



<sup>a</sup>(a) (i) (R)-Lactamide,  $\text{Et}_3\text{O}^+\text{BF}_4^-$ , THF, rt, 2.0 h; (ii) (S)-**451**, EtOH, 75 °C, 3 h (65% over 2 steps); (iii) 3,4-dihydro-2H-pyran, p-TSA, THF, 65 °C, 16 h (87%); (b) (i) For **89** - **86**, (±)-cis-2-(3-fluoro-4-methoxypiperidin-1-yl)pyrimidin-4-ylamine **87**, XPhos,  $\text{Pd}_2(\text{dba})_3$ ,  $\text{Cs}_2\text{CO}_3$ , 1,4-dioxane, 100 °C, 4 h (70%); (ii) For **90** - **86**, (±)-cis-1-(4-aminopyrimidin-2-yl)-3-fluoropiperidin-4-ol **88**, XPhos,  $\text{Pd}_2(\text{dba})_3$ ,  $\text{Cs}_2\text{CO}_3$ , 110 °C, 5 h (49%); (iii) For **89a** - **86**, (-)-2-((3R,4S)-3-fluoro-4-methoxypiperidin-1-yl)pyrimidin-4-ylamine **87a**, XPhos,  $\text{Pd}_2(\text{dba})_3 \cdot \text{CHCl}_3$ ,  $\text{Cs}_2\text{CO}_3$ , 1,4-dioxane, 100 °C, 1.5 h (53%); (iv) For **89b** - **86**, (+)-2-((3S,4R)-3-fluoro-4-methoxypiperidin-1-yl)pyrimidin-4-ylamine **87b**, XPhos,  $\text{Pd}_2(\text{dba})_3 \cdot \text{CHCl}_3$ ,  $\text{Cs}_2\text{CO}_3$ , 1,4-dioxane, 100 °C, 1.5 h (48%); (v) For **90a** - **86**, (-)-(3R,4S)-1-(4-aminopyrimidin-2-yl)-3-fluoropiperidin-4-ol **88a**, XPhos,  $\text{Pd}_2(\text{dba})_3 \cdot \text{CHCl}_3$ ,  $\text{Cs}_2\text{CO}_3$ , 1,4-dioxane, 100 °C, 1 h (55%); (vi) For **90b** - **86**, (+)-(3S,4R)-1-(4-aminopyrimidin-2-yl)-3-fluoropiperidin-4-ol **88b**, XPhos,  $\text{Pd}_2(\text{dba})_3 \cdot \text{CHCl}_3$ ,  $\text{Cs}_2\text{CO}_3$ , 1,4-dioxane, 100 °C, 1 h (44%); (c) For **41a/b**, **42**, **42a/b** - **89a/b**, **90**, **90a/b**, 1.25 M HCl in MeOH, rt, 1-2 h (32-64%); for **41** - **89**, 4M HCl in dioxane, rt, 12 h (73%).

## ASSOCIATED CONTENT

### Supporting information

Kinase profiling data for compounds **2**, **29**, **30**, **17**, **27**, **33**, **42a** and **42b**; tabulated kinase panel and full profiles of compounds **42a** and **42b**; crystallographic data collection and refinement

1  
2  
3 statistics; molecular modeling methods; in vivo xenograft pharmacodynamic studies materials  
4  
5 and methods; experimental details for solubility experiments; experimental details for the  
6  
7 preparation of all compounds; experimental conditions for LC-MS analyses; fluorine NMR  
8  
9 spectra; NMR spectra for key compounds. This material is available free of charge via the  
10  
11 Internet at <http://pubs.acs.org>.  
12  
13

#### 14 15 ACCESSION CODES

16  
17 TMLR/1: 5C8K; TMLR/17: 5C8M; TMLR/23: 5C8N; TMLR/24: 5CAL; TMLR/27: 5CAN;  
18  
19 TMLR/29: 5CAO; TMLR/30: 5CAP; TMLR/33: 5CAQ; wtEGFR/41a: 5CAV; TMLR/41a:  
20  
21 5CAS; TMLR/41b: 5CAU.  
22  
23

#### 24 25 AUTHOR INFORMATION

##### 26 27 **Corresponding Author**

28  
29 \*E-mail: Robert.Heald@crl.com; Phone: +441279 645645  
30  
31

##### 32 33 **Notes**

34  
35 The authors declare no competing financial interest.  
36  
37

##### 38 39 **Author Contributions**

40  
41 The manuscript was written through contributions of all authors. All authors have given  
42  
43 approval to the final version of the manuscript.  
44  
45

#### 46 47 ACKNOWLEDGMENT

48  
49 The authors thank Crystallographic Consulting LLC and Shamrock Structures LLC for  
50  
51 diffraction data collection services and Ping Wu for assistance with some crystals. The Advanced  
52  
53 Light Source (ALS) is supported by the Director, Office of Science, Office of Basic Energy  
54  
55 Sciences, of the U.S. Department of Energy under Contract No. DE-AC0205CH11231. The  
56  
57  
58  
59  
60

1  
2  
3 Berkeley Center for Structural Biology is supported in part by the National Institutes of Health,  
4  
5  
6 National Institute of General Medical Sciences, and the Howard Hughes Medical Institute. The  
7  
8 Advanced Photon Source (APS), an Office of Science User Facility operated for the U.S.  
9  
10 Department of Energy Office of Science by Argonne National Laboratory, was supported by the  
11  
12 U.S. DOE under Contract No. DE-AC02-06CH11357. Use of LS-CAT Sector 21 was supported  
13  
14 by the Michigan Economic Development Corp. and the Michigan Technology Tri-Corridor  
15  
16 (Grant 085P1000817). Use of the IMCA-CAT beamline 17-ID at APS was supported by the  
17  
18 companies of the Industrial Macromolecular Crystallography Association through a contract with  
19  
20 Hauptman-Woodward Medical Research Institute. Use of the Stanford Synchrotron Radiation  
21  
22 Lightsource (SSRL), SLAC National Accelerator Laboratory, is supported by the U.S.  
23  
24 Department of Energy, Office of Science, Office of Basic Energy Sciences under Contract No.  
25  
26 DE-AC02-76SF00515. The SSRL Structural Molecular Biology Program is supported by the  
27  
28 DOE Office of Biological and Environmental Research, and by the National Institutes of Health,  
29  
30 National Institute of General Medical Sciences (including P41GM103393). Research described  
31  
32 in this paper was performed at the Canadian Light Source (CLS), which is funded by the Canada  
33  
34 Foundation for Innovation, the Natural Sciences and Engineering Research Council of Canada,  
35  
36 the National Research Council Canada, the Canadian Institutes of Health Research, the  
37  
38 Government of Saskatchewan, Western Economic Diversification Canada, and the University of  
39  
40 Saskatchewan. The authors thank the analytics group at Argenta for SFC separation of  
41  
42 stereoisomers, ee determination and assignment of NMR spectra. The authors thank Baiwei Lin  
43  
44 for conducting LogD experiments, and thank Savita Ubhayakar, Xiaorong Liang, Ning Liu,  
45  
46 Quynh Ho, and Kirsten Messick for in vitro and in vivo PK and bioanalytical support.  
47  
48  
49  
50  
51  
52  
53  
54  
55  
56  
57  
58  
59  
60

## ABBREVIATIONS

AO, aldehyde oxidase; BrettPhos, 2-(Dicyclohexylphosphino)3,6-dimethoxy-2',4',6'-triisopropyl-1,1'-biphenyl; CDI, 1,1'-carbonyldiimidazole; Cl<sub>hep</sub>, predicted hepatic clearance; Cl<sub>p</sub>, plasma clearance; Cl<sub>u</sub>, free clearance; DIPEA, N,N-diisopropylethylamine; EGFR, epidermal growth factor receptor; wtEGFR, wild-type epidermal growth factor receptor; HATU, 1-[Bis(dimethylamino)methylene]-1H-1,2,3-triazolo[4,5-b]pyridinium 3-oxid hexafluorophosphate; HH, human hepatocyte; HLM, human liver microsome; IP, intraperitoneally; IPA, isopropanol; IVIVC, in vitro in vivo correlation; LLE, lipophilic ligand efficiency; MDCK, Madin-Darby canine kidney; NSCLC, non-small cell lung cancer; Pd<sub>2</sub>(dba)<sub>3</sub>, tris(dibenzylideneacetone)dipalladium(0); RLM, rat liver microsome; RH, rat hepatocyte; SD, standard deviation; p-TSA, p-Toluenesulfonic acid monohydrate; SFC, supercritical fluid chromatography; TKI, tyrosine kinase inhibitor; TMdel, epidermal growth factor receptor (T790M/del746-750); TMLR, epidermal growth factor receptor (T790M/L858R); UPLC, ultra performance liquid chromatography; XO, xanthine oxidase; XPhos, 2-Dicyclohexylphosphino-2',4',6'-triisopropylbiphenyl.

## EXPERIMENTAL SECTION

**Synthesis.** General methods: <sup>1</sup>H NMR spectra were recorded at ambient temperature using either a Varian Unity Inova (400MHz) spectrometer with a triple resonance 5mm probe, an Avance III (300 MHz) spectrometer or a Bruker Ultrashield (400 MHz or 500 MHz) spectrometer. Chemical shifts are expressed in ppm relative to tetramethylsilane. The following abbreviations have been used: br = broad signal, s = singlet, d = doublet, dd = double doublet, t = triplet, q = quartet, m = multiplet. Microwave experiments were carried out using a CEM Discover, Smith Synthesiser or a Biotage Initiator 60™, which uses a single-mode resonator and

dynamic field tuning, both of which give reproducibility and control. Temperatures from 40-250°C can be achieved and pressures of up to 30 bar can be reached. HPLC/UPLC - Mass Spectrometry experiments to determine retention times and associated mass ions were performed using various methods which are fully described in the Supporting Information. All final compounds were assessed for purity by UPLC and found to be  $\geq 95\%$  purity. Diastereomeric and enantiomeric purity of final compounds was assessed by UPLC and SFC respectively and found to be  $>95\%$  de and  $>95\%$  ee.

**(3R,4S)-3-Fluoro-1-{4-[2-((R)-1-hydroxyethyl)-1-((S)-2,2,2-trifluoro-1-methylethyl)-1H-imidazo[4,5 -c]pyridin-6-ylamino]pyrimidin-2-yl}piperidin-4-ol (42a)** (i) **(2-Chloro-5-nitropyridin-4-yl)-((S)-2,2,2-trifluoro-1-methylethyl)amine (44I)** 2,4-Dichloro-5-nitropyridine (11 g, 56.9 mmol), (S)-trifluoromethyl-2-aminopropane (9 g, 79.8 mmol), triethylamine (15.9 mL, 114 mmol) and THF (150 mL) was sealed in a stainless steel pressure vessel and heated at 110°C for 2.5 d. The reaction mixture was diluted with water (~200 mL) and extracted with EtOAc (3 × 100 mL). The combined organic fractions were washed with brine, dried (MgSO<sub>4</sub>) and concentrated *in vacuo*. The resultant residue was purified by flash column chromatography (cyclohexane to EtOAc, 0-50%, gradient elution) to afford the title compound as a dark orange oil (11.9 g, 77%). LCMS (ESI): [M+H]<sup>+</sup> = 270; <sup>1</sup>H NMR (CDCl<sub>3</sub>):  $\delta$  9.08 (1H, s), 8.24 (1H, br s), 6.85 (1H, s), 4.31-4.17 (1H, m), 1.58 (3H, d, J = 6.7 Hz).

**(ii) 6-Chloro-N\*4\*-((S)-2,2,2-trifluoro-1-methylethyl)pyridine-3,4-diamine (45I)** To a solution of (2-chloro-5-nitropyridin-4-yl)-((S)-2,2,2-trifluoro-1-methylethyl)amine **44I** (24 g, 89.0 mmol), acetic acid (24 mL) and water (12 mL) in IMS (250 mL) cooled to ~5°C was added iron powder (29.9 g, 0.53 mol) and the reaction mixture stirred at 5 °C to rt for 2 h (a slight exotherm was observed). The reaction mixture was diluted with EtOAc (~200 mL) and

1  
2  
3 saturated aq. NaHCO<sub>3</sub> added until pH=8. The resultant slurry was filtered through celite and the  
4  
5 solids thoroughly washed with EtOAc. The aqueous fraction was extracted with EtOAc (3 × 100  
6  
7 mL). The combined organic fractions were washed with brine, dried (MgSO<sub>4</sub>) and concentrated  
8  
9 *in vacuo*. The resultant residue was purified by flash column chromatography (cyclohexane to  
10  
11 EtOAc 0-100%, gradient elution) to give the title compound as a dark orange oil which solidified  
12  
13 on standing (17.8 g, 83%). LCMS (ESI): [M+H]<sup>+</sup> = 240.0; <sup>1</sup>H NMR (CDCl<sub>3</sub>): δ 7.74 (1H, s),  
14  
15 6.55 (1H, s), 4.47 (1H, br s), 4.09-3.97 (1H, m), 3.05 (2H, br s), 1.46 (3H, d, J = 6.7 Hz).  
16  
17  
18  
19

20 **(iii) (R)-1-[(S)-6-Chloro-1-(2,2,2-trifluoro-1-methylethyl)-1H-imidazo[4,5-c]pyridin-2-yl]-**  
21  
22 **ethanol (85)** To a suspension of (R)-lactamide (9.86 g, 110.7 mmol) in DCM (300 mL) was  
23  
24 added triethyloxonium tetrafluoroborate (23.2 g, 121.8 mmol) and the reaction mixture stirred at  
25  
26 rt for 2 h, during which the solids dissolved. The reaction mixture was concentrated *in vacuo*  
27  
28 and the resultant residue dissolved in EtOH (400 mL). 6-Chloro-N\*4\*-(S)-2,2,2-trifluoro-1-  
29  
30 methyl-ethyl)-pyridine-3,4-diamine (17.69 g, 73.8 mmol) was added and the reaction mixture  
31  
32 heated at 75 °C for 3 h. The reaction mixture was concentrated *in vacuo* to ~1/3 volume and  
33  
34 diluted with EtOAc (300 mL). The solution was washed with water, then brine, dried (MgSO<sub>4</sub>)  
35  
36 and concentrated *in vacuo*. The resultant residue was purified by flash column chromatography  
37  
38 (cyclohexane to EtOAc 0-100%, gradient elution) to give the title compound as a pale orange  
39  
40 solid (14.08 g, 65%). LCMS (ESI): [M+H]<sup>+</sup> = 294.0; <sup>1</sup>H NMR (CDCl<sub>3</sub>): δ 8.76 (1H, s), 7.48  
41  
42 (1H, s), 5.73-5.51 (1H, m), 5.22 (1H, quin, J = 6.52 Hz), 3.27 (1H, br s), 1.83 (3H, d, J = 7.2 Hz),  
43  
44 1.76 (3H, d, J = 6.8 Hz).  
45  
46  
47  
48  
49

50 **(iv) 6-Chloro-2-[(R)-1-(tetrahydropyran-2-yloxy)ethyl]-1-(2,2,2-trifluoro-1-methylethyl)-**  
51  
52 **1H-imidazo[4,5-c]pyridine (86)** To a solution of (R)-1-[(S)-6-chloro-1-(2,2,2-trifluoro-1-  
53  
54 methylethyl)-1H-imidazo[4,5-c]pyridin-2-yl]ethanol **85** (14.08 g, 47.9 mmol) in THF (200 mL)  
55  
56  
57  
58  
59  
60

1  
2  
3 was added 3,4-dihydro-2H-pyran (35 mL, 0.38 mol) and p-toluenesulfonic acid (911 mg, 4.8  
4 mmol) and the reaction mixture heated at 65 °C for 16 h. The reaction mixture was diluted with  
5 saturated. aq. NaHCO<sub>3</sub> and the product extracted with EtOAc (3 × 80 mL). The combined  
6 organic fractions were washed with brine, dried (MgSO<sub>4</sub>) and concentrated *in vacuo*. The  
7 resultant residue was purified by flash column chromatography (cyclohexane to EtOAc 0-100%,  
8 gradient elution) to give the title compound as a ~1:1 mix of diastereoisomers (15.7 g, 87%).  
9  
10 LCMS (ESI): [M+H]<sup>+</sup> 378.0; <sup>1</sup>H NMR (CDCl<sub>3</sub>): δ 8.84 (1H, s), 8.82 (0.8 H, s), 7.48 (1.8 H, s),  
11 6.02 (1H, sept, J = 7.7 Hz), 5.67 (0.8 H, sept, 7.6 Hz), 5.36-5.21 (1.8 H, m), 4.73 (1H, dd, J =  
12 7.9, 2.6 Hz), 4.61-4.53 (0.8H, m), 3.98-3.78 (1.8H, m), 3.58-3.46 (1.8H, m), 1.89-1.67 (12.6 H,  
13 m), 1.61-1.36 (9 H, m).  
14  
15  
16  
17  
18  
19  
20  
21  
22  
23  
24  
25

26  
27 (v) (-)-(3*R*,4*S*)-1-(4-Aminopyrimidin-2-yl)-3-fluoropiperidin-4-ol (88a) (-)-(3*R*,4*S*)-3-  
28 Fluoro-4-hydroxypiperidine-1-carboxylic acid *tert*-butyl ester (WO2011/36576) (500 mg, 2.27  
29 mmol), was dissolved in HCl in dioxane (4 M, 5 mL) and the reaction stirred at 40 °C  
30 for 90 min. The reaction mixture was concentrated *in vacuo*. The resultant residue was  
31 suspended in IPA (5 mL) and 2-chloro-pyrimidin-4-ylamine (294 mg, 2.27 mmol) and  
32 triethylamine (0.95 mL, 6.82 mmol) were added. The reaction mixture was heated in a sealed  
33 reaction vessel at 130 °C for 16 h and cooled to room temperature. The reaction was  
34 concentrated *in vacuo* and subjected to flash column chromatography (EtOAc/MeOH 100:0 to  
35 90:10, gradient elution) to afford the title compound (383 mg, 79%). LCMS (ESI): [M+H]<sup>+</sup> =  
36 213; [α]<sub>D</sub> -6.8 (c = 3.5, methanol).  
37  
38  
39  
40  
41  
42  
43  
44  
45  
46  
47  
48  
49

50 (vi) (3*R*,4*S*)-3-Fluoro-1-{4-[2-[(*R*)-1-(tetrahydropyran-2-yloxy)ethyl]-1-((*S*)-2,2,2-  
51 trifluoro-1-methylethyl)-1*H*-imidazo[4,5 -*c*]pyridin-6-ylamino]pyrimidin-2-yl}piperidin-4-  
52 ol (90a) 6-Chloro-2-[(*R*)-1-(tetrahydropyran-2-yloxy)ethyl]-1-((*S*)-2,2,2-trifluoro-1-  
53  
54  
55  
56  
57  
58  
59  
60

1  
2  
3 methylethyl)-1*H*-imidazo[4,5 -*c*]pyridine **86** (200 mg, 0.53 mmol), (-)-(3*R*,4*S*)-1-(4-  
4 aminopyrimidin-2-yl)-3-fluoropiperidin-4-ol **88a** (112 mg, 0.53 mmol), 2-  
5 dicyclohexylphosphino-2',4',6'-triisopropylbiphenyl (XPhos, 50 mg, 0.119 mmol), Pd<sub>2</sub>(dba)<sub>3</sub> (27  
6 mg, 0.03 mmol) and Cs<sub>2</sub>CO<sub>3</sub> (345 mg, 1.06 mmol) were suspended in dioxane (5 mL) and the  
7 resultant mixture degassed with argon. The reaction mixture was heated at 100 °C for 1 h. The  
8 reaction mixture was diluted with water and the product extracted with EtOAc (3 × 15 mL). The  
9 combined organic extracts were washed with brine, dried over anhydrous MgSO<sub>4</sub> and  
10 concentrated *in vacuo*. The resultant residue was purified by flash column chromatography on  
11 silica (EtOAc/MeOH 100:0 to 90:10, gradient elution) to yield the title compound (160 mg,  
12 55%) LCMS (ESI): [M+H]<sup>+</sup> = 554.0.

13  
14  
15  
16  
17  
18  
19  
20  
21  
22  
23  
24  
25  
26  
27 (vii) (3*R*,4*S*)-3-Fluoro-1-{4-[2-((*R*)-1-hydroxyethyl)-1-((*S*)-2,2,2-trifluoro-1-methylethyl)-  
28 1*H*-imidazo[4,5 -*c*]pyridin-6-ylamino]pyrimidin-2-yl}piperidin-4-ol (**42a**) (3*R*,4*S*)-3-Fluoro-  
29 1-{4-[2-[(*R*)-1-(tetrahydropyran-2-yloxy)ethyl]-1-((*S*)-2,2,2-trifluoro-1-methylethyl)-1*H*-  
30 imidazo[4,5-*c*]pyridin-6-ylamino]pyrimidin-2-yl}piperidin-4-ol **90a** (160 mg, 0.29 mmol) was  
31 dissolved in HCl in MeOH (1.25 M, 5 mL) and the reaction mixture was stirred at room  
32 temperature for 3 h. The reaction mixture was diluted with saturated aq. NaHCO<sub>3</sub> and the  
33 product extracted with EtOAc (3 × 15 mL). The combined organic extracts were washed with  
34 brine, dried over anhydrous MgSO<sub>4</sub> and concentrated *in vacuo*. The resultant residue was  
35 subjected to preparative HPLC to yield the title compound as a white solid (53 mg, 39%).  
36 LCMS (ESI): rt 2.28 min, [M+H]<sup>+</sup> 470.0, Method = 3; <sup>1</sup>H NMR 400MHz δ (d<sub>6</sub>-DMSO): 9.80  
37 (1H, br s), 8.63 (1H, s), 8.32 (1H, br s), 7.93 (1H, d, J = 5.9 Hz), 6.44 (1H, br s), 5.91 (1H, d, J =  
38 6.2 Hz), 5.90-5.78 (1H, m), 5.07 (1H, d, J = 5.3), 4.98 (1H, quin, J = 6.6 Hz), 4.69-4.65 (0.5H,  
39  
40  
41  
42  
43  
44  
45  
46  
47  
48  
49  
50  
51  
52  
53  
54  
55  
56  
57  
58  
59  
60

m), 4.58-4.49 (1.5H, m), 4.34-4.26 (1H, m), 3.86-3.72 (1H, m), 3.49-3.40 (1H, m), 1.81 (3H, d, J = 7.1 Hz), 1.68-1.60 (3H, m), 1.58 (3H, d, J = 6.6 Hz).

**(3*S*,4*R*)-3-Fluoro-1-{4-[2-((*R*)-1-hydroxyethyl)-1-((*S*)-2,2,2-trifluoro-1-methylethyl)-1*H*-imidazo[4,5-*c*]pyridin-6-ylamino]pyrimidin-2-yl}piperidin-4-ol (42b)**

**(i) (+)-(3*S*,4*R*)-1-(4-Aminopyrimidin-2-yl)-3-fluoropiperidin-4-ol (88b)** (+)-(3*S*,4*R*)-3-fluoro-4-hydroxypiperidine-1-carboxylic acid *tert*-butyl ester (500 mg, 2.27 mmol), was dissolved in HCl in dioxane (4 M, 5 mL) and the reaction stirred at 40 °C for 90 min. The reaction mixture was concentrated *in vacuo*. The resultant residue was suspended in IPA (5 mL) and 2-chloro-pyrimidin-4-ylamine (294 mg, 2.27 mmol) and triethylamine (0.95 mL, 6.82 mmol) added. The reaction mixture was heated in a sealed vial at 130 °C for 16 h. The reaction mixture was concentrated *in vacuo* and purified by flash column chromatography (EtOAc/MeOH 100:0 to 90:10, gradient elution) to yield the title compound (378 mg, 78%). LCMS (ESI): [M+H]<sup>+</sup> = 213.0; [α]<sub>D</sub> +9.0° (c = 3.5 in methanol).

**(ii) (3*S*,4*R*)-3-Fluoro-1-{4-[2-[(*R*)-1-(tetrahydropyran-2-yloxy)ethyl]-1-((*S*)-2,2,2-trifluoro-1-methylethyl)-1*H*-imidazo[4,5-*c*]pyridin-6-ylamino]pyrimidin-2-yl}piperidin-4-ol (90b)** 6-Chloro-2-[(*R*)-1-(tetrahydropyran-2-yloxy)ethyl]-1-((*S*)-2,2,2-trifluoro-1-methylethyl)-1*H*-imidazo[4,5-*c*]pyridine **86** (200 mg, 0.53 mmol), (+)-(3*S*,4*R*)-1-(4-aminopyrimidin-2-yl)-3-fluoropiperidin-4-ol **88b** (112 mg, 0.53 mmol), 2-dicyclohexylphosphino-2',4',6'-triisopropylbiphenyl (50 mg, 0.119 mmol), Pd<sub>2</sub>dba<sub>3</sub> (27 mg, 0.03 mmol) and Cs<sub>2</sub>CO<sub>3</sub> (345 mg, 1.06 mmol) were suspended in dioxane (5 mL) and the resultant mixture degassed with argon. The reaction mixture was heated at 100 °C for 1 h. The reaction mixture was diluted with water and extracted with EtOAc (3 × 15 mL). The combined organic extracts were washed with brine, dried over anhydrous MgSO<sub>4</sub> and concentrated *in vacuo*. The

1  
2  
3 resultant residue was purified by flash column chromatography (EtOAc/MeOH 100:0 to 90:10,  
4  
5 gradient elution) to afford the title compound (150 mg, 44%) LCMS (ESI):  $[M+H]^+ = 554.0$ .

6  
7  
8 (iii) (3*S*,4*R*)-3-Fluoro-1-{4-[2-((*R*)-1-hydroxyethyl)-1-((*S*)-2,2,2-trifluoro-1-methylethyl)-  
9  
10 1*H*-imidazo[4,5-*c*]pyridin-6-ylamino]pyrimidin-2-yl}piperidin-4-ol (42b) (3*S*,4*R*)-3-Fluoro-  
11  
12 1-{4-[2-[(*R*)-1-(tetrahydropyran-2-yloxy)ethyl]-1-((*S*)-2,2,2-trifluoro-1-methylethyl)-1*H*-  
13  
14 imidazo[4,5-*c*]pyridin-6-ylamino]pyrimidin-2-yl}piperidin-4-ol 90b (150 mg, 0.27 mmol) was  
15  
16 dissolved in HCl in MeOH (5 mL, 1.25 M) and the reaction mixture was stirred at room  
17  
18 temperature for 3 h. The reaction mixture was diluted with saturated aq. NaHCO<sub>3</sub> and extracted  
19  
20 with EtOAc (3 × 15 mL). The combined organic extracts were washed with brine, dried over  
21  
22 anhydrous MgSO<sub>4</sub> and concentrated *in vacuo*. The resultant residue was subjected to preparative  
23  
24 HPLC to yield the title compound as a white solid (53 mg, 39%). LCMS (ESI): *rt* = 2.28 min,  
25  
26  $[M+H]^+ = 470$ , Method = 3; <sup>1</sup>H NMR 400MHz  $\delta$  (d<sub>6</sub>-DMSO): 9.80 (1H, br s), 8.63 (1H, s), 8.31  
27  
28 (1H, br s), 7.93 (1H, d, *J* = 5.9 Hz), 6.44 (1H, br s), 5.91 (1H, d, *J* = 6.2 Hz), 5.90-5.76 (1H, m),  
29  
30 5.11-5.04 (1H, m), 4.98 (1H, quin, *J* = 6.6 Hz), 4.68-4.64 (0.5H, m), 4.56-4.44 (1.5H, m), 4.34-  
31  
32 4.24 (1H, m), 3.86-3.72 (1H, m), 3.53-3.40 (1H, m), 1.81 (3H, d, *J* = 7.1 Hz), 1.71-1.60 (3H, m),  
33  
34 1.58 (3H, d, *J* = 6.6 Hz).

35  
36  
37  
38  
39  
40  
41 **Enzymatic assays** were carried out as previously described.<sup>70</sup> All enzymatic data reported are  
42  
43 the average of at least two independent experiments, data were only reported when repeat  
44  
45 determinations were within 2-fold and the control (AZD7662) was within 3-fold of historical  
46  
47 average. Control values, geometric mean  $\pm$  standard deviation: TMLR  $K_{iapp} = 18 \pm 7.8$  nM;  
48  
49 TMdel  $K_{iapp} = 4.6 \pm 1.8$  nM; WT  $K_{iapp} = 29 \pm 9$  nM.

50  
51  
52  
53 **H1975, H292 and PC9 pEGFR MSD Cellular Assays.** These assays were used for  
54  
55 determining cellular potency of mutant-selective EGFR small molecule inhibitors. The potency  
56  
57  
58  
59  
60

1  
2  
3 of compounds to inhibit phosphor-EGFR in the following EGFR expressing cell lines was  
4 determined using the Meso Scale Discovery 384 well pEGFR Tyr1068 assay kits. (Meso Scale  
5 Discovery Catalog# N31CB-1). NCI-H1975 (ATCC Catalog# CRL-5908), EGFR  
6 T790M/L858R. PC9-ER (generated at Genentech), EGFR ex19del + T790M. Generation of  
7 PC9 erlotinib resistant line (PC9-ER): PC9 cells were treated with 2  $\mu$ M erlotinib. Media was  
8 replaced every 3 to 4 days with new media containing 2  $\mu$ M of erlotinib. After 2 months viable  
9 cells were collected as a 2  $\mu$ M erlotinib-resistant pool. The erlotinib concentration was gradually  
10 increased from 2- 10  $\mu$ M. PC9 cells grown for a month in 10  $\mu$ M erlotinib were designated PC9-  
11 ER cells. NCI-H292 (ATCC Catalog# CRL-1848), EGFR WT. Cell Culture: NCI-H1975 and  
12 NCI-H292 cells were separately maintained in medium containing RPMI 1640, 10% FBS, 4 mM  
13 L-Glutamine, 1% Penicillin-Streptomycin, and 4.5 g/L glucose. All cell culture reagents were  
14 purchased from Invitrogen/Gibco. Cells were cultured at 37 °C at 5% CO<sub>2</sub> and split as  
15 recommended by ATCC. PC9-ER cells were maintained in medium containing RPMI 1640,  
16 10% FBS, 4 mM L-Glutamine, and 10  $\mu$ M Erlotinib. Cells are cultured at 37 °C at 5% CO<sub>2</sub> and  
17 maintained at a sub-confluent density by harvesting with trypsin and sub culturing at a ratio of  
18 1:8 every 72 h. Cell Plating and Serum Starvation: NCI-H1975, NCI-H292, or PC9-ER cells  
19 were harvested and plated into sterile cell culture treated 384 well plates (Greiner catalog  
20 #781091) at a density of 30,000 cells/well in 50  $\mu$ L culture medium and placed in a 37 °C at 5%  
21 CO<sub>2</sub> incubator for 6 h. After 6 h, culture medium was aspirated and replaced with serum-free  
22 culture medium. Cells were then incubated with the serum-free medium overnight at 37 °C and  
23 5% CO<sub>2</sub>. Assay Procedure: The following day, test compounds were serially diluted in dimethyl  
24 sulfoxide (DMSO) and added to cells in serum free medium (final DMSO concentration 0.5%).  
25 Assay plates were then incubated for 1 hour at 37 °C and 5% CO<sub>2</sub>. Following compound  
26  
27  
28  
29  
30  
31  
32  
33  
34  
35  
36  
37  
38  
39  
40  
41  
42  
43  
44  
45  
46  
47  
48  
49  
50  
51  
52  
53  
54  
55  
56  
57  
58  
59  
60

1  
2  
3 incubation for 1 h, H292 WT cells were stimulated with 100 ng/ml EGF for 8 minutes. All cells  
4  
5 were then lysed and processed as per the MSD pEGFR assay kit protocol. Cell lysates were  
6  
7 added to assay plates pre-coated with antibodies against phosphorylated EGFR. Phosphorylated  
8  
9 EGFR in samples are allowed to bind to the capture antibodies overnight at 4 °C. The detection  
10  
11 antibody (anti-total EGFR, labeled with an electrochemiluminescent SULFO-TAG) was added to  
12  
13 the bound lysate and incubated for 1 h at room temperature. The MSD Read Buffer was added  
14  
15 such that when a voltage is applied to the plate electrodes, the labels bound to the electrode  
16  
17 surface emit light. The MSD Sector Instrument measures the intensity of the light, and  
18  
19 quantitatively measures the amount of phosphorylated-EGFR in the sample. Percent inhibition  
20  
21 of EGFR phosphorylation by varying concentrations of test compounds was calculated relative to  
22  
23 untreated controls. EC<sub>50</sub> values were calculated using the 4 parameter logistic nonlinear  
24  
25 regression dose-response model. All values quoted are the average of at least two independent  
26  
27 experiments, data were only reported when repeat determinations were within 2-fold and the  
28  
29 control was within 3-fold of historical average.  
30  
31  
32  
33  
34  
35  
36  
37  
38

39 **H1975, H292, and PC9-ER Proliferation Assays.** These assays were used to determine the  
40  
41 potency of compounds to inhibit H1975 (EGFR T790M/L858R), NCI-H292 (EGFR WT), and  
42  
43 PC9-ER (EGFR ex19del + T790M) cell proliferation. Cell Culture: NCI-H1975 and NCI-H292  
44  
45 cells both separately maintained in medium containing RPMI 1640, 10% FBS, 4 mM L-  
46  
47 Glutamine, 1% Penicillin-Streptomycin, and 4.5 g/L glucose. All cell culture reagents were  
48  
49 purchased from Invitrogen/Gibco. Cells were cultured at 37 °C at 5% CO<sub>2</sub> and split as  
50  
51 recommended by ATCC. PC9-ER cells were maintained in medium containing RPMI 1640,  
52  
53 10% FBS, 4 mM L-Glutamine, and 10 μM erlotinib. Cells were cultured at 37 °C at 5% CO<sub>2</sub> and  
54  
55  
56  
57  
58  
59  
60

1  
2  
3 maintained at a sub-confluent density by harvesting with trypsin and sub culturing at a ratio of  
4 1:8 every 72 h. Assay Procedure: NCI-H1975 or NCI-H292 cells were harvested and plated into  
5 sterile cell culture treated 384 well plates (Greiner catalog #781091) at a density of 1000  
6 cells/well in 50  $\mu$ L culture medium and placed in a 37  $^{\circ}$ C at 5% CO<sub>2</sub> incubator overnight. PC9-  
7 ER cells were harvested and plated into sterile cell culture treated 384 well plates (Greiner  
8 catalog #781091) at a density of 1000 cells/well in 50  $\mu$ L culture medium including 10  $\mu$ M  
9 erlotinib and placed in a 37  $^{\circ}$ C at 5% CO<sub>2</sub> incubator overnight. The following day, test  
10 compounds were serially diluted in dimethyl sulfoxide (DMSO) and added to cells in culture  
11 medium (final DMSO concentration 0.5%, final assay volume 50  $\mu$ L). Assay plates were then  
12 incubated for 72 h at 37  $^{\circ}$ C and 5% CO<sub>2</sub>. After 72 h, 25  $\mu$ L of reconstituted Promega Cell Titer-  
13 Glo reagent (Promega Catalog# G7572) was added to all wells. Plates were then read on a Perkin  
14 Elmer Envision Multi-label plate reader using luminescence mode. Percent inhibition of  
15 proliferation by varying concentrations of test compounds is calculated relative to untreated  
16 controls. EC<sub>50</sub> values were calculated using the 4 parameter logistic nonlinear regression dose-  
17 response model. All values quoted are the average of at least two independent experiments, data  
18 were only reported when repeat determinations were within 2-fold and the control was within 2-  
19 fold of historical average.

20  
21  
22 **Control compounds for cell assays.** Control values shown are geometric mean  $\pm$  standard  
23 deviation. H1975: Compound **42**. pEGFR H1975 IC<sub>50</sub> = 236  $\pm$  9.4 nM; H1975 prolif. EC<sub>50</sub> =  
24 868  $\pm$  310). This control was used due to the lack of selectivity of potent literature compounds  
25 available at the time. Assays for earlier compounds were repeated once compound **42** was  
26 available and found to be consistent. H292: erlotinib. pEGFR H292 IC<sub>50</sub> (nM) 6.3  $\pm$  3.2 nM;  
27 H292 prolif. EC<sub>50</sub> (nM) 31  $\pm$  20 nM. PC9(ER):  
28  
29  
30  
31  
32  
33  
34  
35  
36  
37  
38  
39  
40  
41  
42  
43  
44  
45  
46  
47  
48  
49  
50  
51  
52  
53  
54  
55  
56  
57  
58  
59  
60

1  
2  
3     **Log D determination.** Microscale shake flask log D assay: Test compounds were prepared as  
4  
5 10 mM DMSO stock solutions and stored at room temperature to avoid precipitation that can be  
6  
7 induced by a freeze-thaw cycle. Two buffers were used in the assay: a saturated 1-  
8  
9 octanol/phosphate buffer solution (20 mL PBS pH7.4 + 200 mL 1-octanol) and a saturated  
10  
11 PBS/1-octanol solution (1 mL 1-octanol + 200 mL PBS pH 7.4). Each solution was freshly  
12  
13 prepared, shaken for 1 h and allowed to stand for 24 h before use. The Tecan robot first  
14  
15 dispensed 250  $\mu$ L of the saturated 1-octanol/PBS solution into each well of a 96-deep well plate  
16  
17 and then added 5  $\mu$ L of a 10 mM test compound in DMSO stock solution. The plates were sealed  
18  
19 with aluminum sealing film and shaken for 20 minutes at 1000 rpm. After shaking, the Tecan  
20  
21 added 250  $\mu$ L of saturated PBS/1-octanol solution to each well. The plates were then resealed,  
22  
23 shaken for 1 h at 1000 rpm at room temperature (25°C), and centrifuged at 3000 rpm for 10 min.  
24  
25 Sample analyses were carried out by transferring the octanol and PBS phases to 384 well plates.  
26  
27 Finally, 2  $\mu$ L of 0.1 mM propranolol in acetonitrile was added to each well as an internal  
28  
29 standard. Detection by LC-MS/MS. A UPLC/MS/MS equipped with Shimadzu LC and Sciex  
30  
31 API4000 was used for quantification of octanol and PBS samples. The quantification was  
32  
33 performed by MRM (multiple reaction monitor) transition analysis. With separate injections, 3  
34  
35  $\mu$ L for the octanol samples and 10  $\mu$ L for the PBS samples, MRM peaks were collected,  
36  
37 processed, and integrated. The lipophilicity of the compound was determined as the log of ratio  
38  
39 of MRM peaks in octanol and PBS phases. Measured LogD values reported are average of at  
40  
41 least two separate determinations.  
42  
43  
44  
45  
46  
47  
48  
49

50     **cLogP calculation.** MoKa software (version 1.1.0, Molecular Discovery) was used to  
51  
52 calculate the logarithm of the partition coefficient (cLogP).  
53  
54

55     **Kinetic solubility.** Solubility determination was as previously described.<sup>39</sup>  
56  
57  
58  
59  
60

1  
2  
3 **In vitro microsome and hepatocyte metabolic stability assays.** Experiments were carried  
4 out as previously described.<sup>71,72</sup> Values shown are for predicted hepatic clearance using intrinsic  
5 clearance and a conversion factor for liver blood flow to predict hepatic clearance.  $Cl_{hep} =$   
6  $(Q \cdot Cl_{int}) / (Q + Cl_{int})$  where  $Cl_{hep}$  = predicted hepatic clearance,  $Q$  = liver blood flow and  $Cl_{int}$  =  
7 intrinsic clearance. Liver blood flow values in mL/min/kg rat = 55.2, dog = 30.9, human = 20.7,  
8 mouse = 90.  
9

10  
11 **X-ray crystallography.** Crystallographic methods and the production and use of TMLR  
12 proteins were as previously described<sup>39</sup>. For the wild-type EGFR kinase domain, codon  
13 optimized DNA encoding residues Gly696-Gln1021 and an N-terminal His6-tag and TEV  
14 cleavage site were cloned into a modified version of BD Pharmingen pAcGP67 vector. Sf9 cells  
15 were used for virus generation and expression. After harvest, cells were resuspended in a buffer  
16 containing of 600 mM NaCl, 15% glycerol, 50 mM Tris-HCl pH7.5, 1 mM TCEP supplemented  
17 with a protease-inhibitor cocktail (Complete EDTA-free, Roche), homogenized and lysed by  
18 Microfluidizer and centrifuged at 186000xg for 1hr at 4°C. The clear supernatant was filtered  
19 and loaded onto Nickel-chelating resin (Qiagen). EGFR protein was eluted with 25 mM Tris-  
20 HCl pH 8.0, 500 mM NaCl, 10% glycerol, 250 mM imidazole and 1 mM TCEP. The His6-tag  
21 was removed by dialysis with TEV Protease overnight at 4°C in 50mM Tris-HCl pH8, 250 mM  
22 NaCl, 10% glycerol and 1 mM TCEP, followed by a second nickel affinity column capturing the  
23 flow-through. Apo-EGFR was concentrated and further purified over a HiLoad 16/60 Superdex  
24 75 size-exclusion column (GE Healthcare) in 500 mM NaCl, 50 mM Tris-HCl pH 8.0, 10%  
25 glycerol and 1mM TCEP. Final unphosphorylated EGFR protein was concentrated to ~10 – 12  
26 mg/mL in the final buffer of 25 mM Tris-HCl pH 8.0, 100 mM NaCl, 2 mM DTT, 2 mM TCEP.  
27 Crystals were grown at 19°C by the hanging-drop vapor diffusion method described in Stamos et  
28  
29  
30  
31  
32  
33  
34  
35  
36  
37  
38  
39  
40  
41  
42  
43  
44  
45  
46  
47  
48  
49  
50  
51  
52  
53  
54  
55  
56  
57  
58  
59  
60

1  
2  
3 al.<sup>73</sup> Purified wild-type EGFR kinase domain was crystallized in 1:1 ratio (2.5 $\mu$ l protein: 2.5 $\mu$ l  
4 well solution) containing 1M Na/K tartrate, 0.1M Mes pH7. Crystals formed after overnight at  
5  
6 19°C. The inhibitor-bound complex of EGFR was prepared by diffusion soaking from 1.0 mM  
7  
8 to 2.5 mM inhibitor plus well solution into apo EGFR crystals using microbridges (Hampton  
9  
10 Research) and incubated at 19°C for 2 days. Crystals were cryoprotected in well solution  
11  
12 supplemented with 20% glycerol before immersion in liquid nitrogen.  
13  
14  
15  
16

## 17 REFERENCES

- 18 1. Gazdar, A. F.; Minna, J. D. Inhibition of EGFR signaling: all mutations are not created  
19 equal. *PLoS Med* **2005**, *2*, e377.
- 20 2. Sharma, S. V.; Bell, D. W.; Settleman, J.; Haber, D. A. Epidermal growth factor receptor  
21 mutations in lung cancer. *Nat Rev Cancer* **2007**, *7*, 169-81.
- 22 3. Sordella, R.; Bell, D. W.; Haber, D. A.; Settleman, J. Gefitinib-sensitizing EGFR  
23 mutations in lung cancer activate anti-apoptotic pathways. *Science* **2004**, *305*, 1163-7.
- 24 4. Tracy, S.; Mukohara, T.; Hansen, M.; Meyerson, M.; Johnson, B. E.; Janne, P. A.  
25 Gefitinib induces apoptosis in the EGFR<sup>L858R</sup> non-small-cell lung cancer cell line H3255.  
26 *Cancer Res* **2004**, *64*, 7241-4.
- 27 5. Sharma, S. V.; Settleman, J. Oncogene addiction: setting the stage for molecularly  
28 targeted cancer therapy. *Genes Dev* **2007**, *21*, 3214-31.
- 29 6. Jackman, D. M.; Miller, V. A.; Cioffredi, L. A.; Yeap, B. Y.; Janne, P. A.; Riely, G. J.;  
30 Ruiz, M. G.; Giaccone, G.; Sequist, L. V.; Johnson, B. E. Impact of epidermal growth factor  
31 receptor and KRAS mutations on clinical outcomes in previously untreated non-small cell lung  
32 cancer patients: results of an online tumor registry of clinical trials. *Clin Cancer Res* **2009**, *15*,  
33 5267-73.
- 34 7. Rosell, R.; Moran, T.; Queralt, C.; Porta, R.; Cardenal, F.; Camps, C.; Majem, M.;  
35 Lopez-Vivanco, G.; Isla, D.; Provencio, M.; Insa, A.; Massuti, B.; Gonzalez-Larriba, J. L.; Paz-  
36 Ares, L.; Bover, I.; Garcia-Campelo, R.; Moreno, M. A.; Catot, S.; Rolfó, C.; Reguart, N.;  
37 Palmero, R.; Sanchez, J. M.; Bastus, R.; Mayo, C.; Bertran-Alamillo, J.; Molina, M. A.; Sanchez,  
38 J. J.; Taron, M. Screening for epidermal growth factor receptor mutations in lung cancer. *N Engl*  
39 *J Med* **2009**, *361*, 958-67.
- 40 8. Lynch, T. J.; Bell, D. W.; Sordella, R.; Gurubhagavatula, S.; Okimoto, R. A.; Brannigan,  
41 B. W.; Harris, P. L.; Haserlat, S. M.; Supko, J. G.; Haluska, F. G.; Louis, D. N.; Christiani, D.  
42 C.; Settleman, J.; Haber, D. A. Activating mutations in the epidermal growth factor receptor  
43 underlying responsiveness of non-small-cell lung cancer to gefitinib. *N Engl J Med* **2004**, *350*,  
44 2129-39.
- 45 9. Paez, J. G.; Janne, P. A.; Lee, J. C.; Tracy, S.; Greulich, H.; Gabriel, S.; Herman, P.;  
46 Kaye, F. J.; Lindeman, N.; Boggon, T. J.; Naoki, K.; Sasaki, H.; Fujii, Y.; Eck, M. J.; Sellers, W.  
47 R.; Johnson, B. E.; Meyerson, M. EGFR mutations in lung cancer: correlation with clinical  
48 response to gefitinib therapy. *Science* **2004**, *304*, 1497-500.
- 49  
50  
51  
52  
53  
54  
55  
56  
57  
58  
59  
60

- 1  
2  
3  
4  
5  
6  
7  
8  
9  
10  
11  
12  
13  
14  
15  
16  
17  
18  
19  
20  
21  
22  
23  
24  
25  
26  
27  
28  
29  
30  
31  
32  
33  
34  
35  
36  
37  
38  
39  
40  
41  
42  
43  
44  
45  
46  
47  
48  
49  
50  
51  
52  
53  
54  
55  
56  
57  
58  
59  
60
10. Pao, W.; Miller, V.; Zakowski, M.; Doherty, J.; Politi, K.; Sarkaria, I.; Singh, B.; Heelan, R.; Rusch, V.; Fulton, L.; Mardis, E.; Kupfer, D.; Wilson, R.; Kris, M.; Varmus, H. EGF receptor gene mutations are common in lung cancers from "never smokers" and are associated with sensitivity of tumors to gefitinib and erlotinib. *Proc Natl Acad Sci U S A* **2004**, 101, 13306-11.
  11. Pao, W.; Chmielecki, J. Rational, biologically based treatment of EGFR-mutant non-small-cell lung cancer. *Nat Rev Cancer* **2010**, 10, 760-74.
  12. Kobayashi, S.; Boggon, T. J.; Dayaram, T.; Janne, P. A.; Kocher, O.; Meyerson, M.; Johnson, B. E.; Eck, M. J.; Tenen, D. G.; Halmos, B. EGFR mutation and resistance of non-small-cell lung cancer to gefitinib. *N Engl J Med* **2005**, 352, 786-92.
  13. Pao, W.; Miller, V. A.; Politi, K. A.; Riely, G. J.; Somwar, R.; Zakowski, M. F.; Kris, M. G.; Varmus, H. Acquired resistance of lung adenocarcinomas to gefitinib or erlotinib is associated with a second mutation in the EGFR kinase domain. *PLoS Med* **2005**, 2, e73.
  14. Yu, H. A.; Arcila, M. E.; Rekhtman, N.; Sima, C. S.; Zakowski, M. F.; Pao, W.; Kris, M. G.; Miller, V. A.; Ladanyi, M.; Riely, G. J. Analysis of tumor specimens at the time of acquired resistance to EGFR-TKI therapy in 155 patients with EGFR-mutant lung cancers. *Clin Cancer Res* **2013**, 19, 2240-7.
  15. Kosaka, T.; Yatabe, Y.; Endoh, H.; Yoshida, K.; Hida, T.; Tsuboi, M.; Tada, H.; Kuwano, H.; Mitsudomi, T. Analysis of epidermal growth factor receptor gene mutation in patients with non-small cell lung cancer and acquired resistance to gefitinib. *Clin Cancer Res* **2006**, 12, 5764-9.
  16. Balak, M. N.; Gong, Y.; Riely, G. J.; Somwar, R.; Li, A. R.; Zakowski, M. F.; Chiang, A.; Yang, G.; Ouerfelli, O.; Kris, M. G.; Ladanyi, M.; Miller, V. A.; Pao, W. Novel D761Y and common secondary T790M mutations in epidermal growth factor receptor-mutant lung adenocarcinomas with acquired resistance to kinase inhibitors. *Clin Cancer Res* **2006**, 12, 6494-501.
  17. Erlotinib activity in biochemical assays: wtEGFR Ki = 0.1 nM, EGFR(d746-750) Ki = 0.1 nM, EGFR(T790M/L858R) Ki = 123 nM, EGFR(T790M/d746-750) Ki = 95 nM.
  18. Kwak, E. L.; Sordella, R.; Bell, D. W.; Godin-Heymann, N.; Okimoto, R. A.; Brannigan, B. W.; Harris, P. L.; Driscoll, D. R.; Fidias, P.; Lynch, T. J.; Rabindran, S. K.; McGinnis, J. P.; Wissner, A.; Sharma, S. V.; Isselbacher, K. J.; Settleman, J.; Haber, D. A. Irreversible inhibitors of the EGF receptor may circumvent acquired resistance to gefitinib. *Proc Natl Acad Sci U S A* **2005**, 102, 7665-70.
  19. Shah, N. P.; Nicoll, J. M.; Nagar, B.; Gorre, M. E.; Paquette, R. L.; Kuriyan, J.; Sawyers, C. L. Multiple BCR-ABL kinase domain mutations confer polyclonal resistance to the tyrosine kinase inhibitor imatinib (STI571) in chronic phase and blast crisis chronic myeloid leukemia. *Cancer Cell* **2002**, 2, 117-25.
  20. Quintas-Cardama, A.; Kantarjian, H.; Cortes, J. Flying under the radar: the new wave of BCR-ABL inhibitors. *Nat Rev Drug Discov* **2007**, 6, 834-48.
  21. Yun, C. H.; Mengwasser, K. E.; Toms, A. V.; Woo, M. S.; Greulich, H.; Wong, K. K.; Meyerson, M.; Eck, M. J. The T790M mutation in EGFR kinase causes drug resistance by increasing the affinity for ATP. *Proc Natl Acad Sci U S A* **2008**, 105, 2070-5.
  22. Janne, P. A.; Schellens, J. H.; Engelman, J. A.; Eckhardt, S. G.; Millham, R.; Denis, L. J.; Britten, C. D.; Wong, S. G.; Boss, D. S.; Camidge, D. R. Preliminary activity and safety results from a phase I clinical trial of PF-00299804, an irreversible pan-HER inhibitor, in patients (pts) with NSCLC. *Journal of Clinical Oncology* **2008**, 26, (May 20 suppl; abstr 8027).

23. Sequist, L. V.; Besse, B.; Lynch, T. J.; Miller, V. A.; Wong, K. K.; Gitlitz, B.; Eaton, K.; Zacharchuk, C.; Freyman, A.; Powell, C.; Ananthkrishnan, R.; Quinn, S.; Soria, J. C. Neratinib, an irreversible pan-ErbB receptor tyrosine kinase inhibitor: results of a phase II trial in patients with advanced non-small-cell lung cancer. *J Clin Oncol* **2010**, *28*, 3076-83.
24. Kim, Y.; Ko, J.; Cui, Z.; Abolhoda, A.; Ahn, J. S.; Ou, S. H.; Ahn, M. J.; Park, K. The EGFR T790M mutation in acquired resistance to an irreversible second-generation EGFR inhibitor. *Mol Cancer Ther* **2012**, *11*, 784-91.
25. Sos, M. L.; Rode, H. B.; Heynck, S.; Peifer, M.; Fischer, F.; Kluter, S.; Pawar, V. G.; Reuter, C.; Heuckmann, J. M.; Weiss, J.; Ruddigkeit, L.; Rabiller, M.; Koker, M.; Simard, J. R.; Getlik, M.; Yuza, Y.; Chen, T. H.; Greulich, H.; Thomas, R. K.; Rauh, D. Chemogenomic profiling provides insights into the limited activity of irreversible EGFR Inhibitors in tumor cells expressing the T790M EGFR resistance mutation. *Cancer Res* **2010**, *70*, 868-74.
26. Soria, J.-C.; Sequist, L. V.; Gadgeel, S.; Goldman, J.; Wakelee, H.; Varga, A.; Fidias, P.; Wozniak, A. J.; Neal, J. W.; Doebele, R. C.; Garon, E. B.; Jaw-Tsai, S.; Caunt, L.; Kaur, P.; Rolfe, L.; Allen, A.; Camidge, D. R. First-in-human evaluation of CO-1686, an irreversible, highly selective tyrosine kinase inhibitor of mutations of EGFR (activating and T790M). In *15th World Conference on Lung Cancer*, Sydney, Australia, 2013.
27. Ranson, M. Preliminary results from a Phase I study with AZD9291. In *European Cancer Congress*, 2013.
28. Cross, D. A. E.; Ashton, S. E.; Ghiorghiu, S.; Eberlein, C.; Nebhan, C. A.; Spitzler, P. J.; Orme, J. P.; Finlay, M. R. V.; Ward, R. A.; Mellor, M. J.; Hughes, G.; Rahi, A.; Jacobs, V. N.; Brewer, M. R.; Ichihara, E.; Sun, J.; Jin, H.; Ballard, P.; Al-Kadhimi, K.; Rowlinson, R.; Klinowska, T.; Richmond, G. H. P.; Cantarini, M.; Kim, D.-W.; Ranson, M. R.; Pao, W. AZD9291, an Irreversible EGFR TKI, Overcomes T790M-Mediated Resistance to EGFR Inhibitors in Lung Cancer. *Cancer Discovery* **2014**, *4*, 1046-1061.
29. Sjin, R. T. T.; Lee, K.; Walter, A. O.; Dubrovskiy, A.; Sheets, M.; Martin, T. S.; Labenski, M. T.; Zhu, Z.; Tester, R.; Karp, R.; Medikonda, A.; Chaturvedi, P.; Ren, Y.; Haringsma, H.; Etter, J.; Raponi, M.; Simmons, A. D.; Harding, T. C.; Niu, D.; Nacht, M.; Westlin, W. F.; Petter, R. C.; Allen, A.; Singh, J. In Vitro and In Vivo Characterization of Irreversible Mutant-Selective EGFR Inhibitors That Are Wild-Type Sparing. *Mol. Cancer Ther.* **2014**, *13*, 1-12.
30. Janne, P. A.; Ramaligam, S. S.; Yang, J. C. H.; Ahn, M.-J.; Kim, D.-W.; Kim, S.-W.; Planchard, D.; Ohe, Y.; Felip, E.; Watkins, C.; Cantarini, M.; Ghiorghiu, S.; Ranson, M. Clinical activity of the mutant-selective EGFR inhibitor AZD9291 in patients (pts) with EGFR inhibitor-resistant non-small-cell lung cancer (NSCLC). *J. Clin. Oncol.* **2014**, *32*, 8009.
31. Jänne, P. A.; Yang, J. C.-H.; Kim, D.-W.; Planchard, D.; Ohe, Y.; Ramalingam, S. S.; Ahn, M.-J.; Kim, S.-W.; Su, W.-C.; Horn, L.; Haggstrom, D.; Felip, E.; Kim, J.-H.; Frewer, P.; Cantarini, M.; Brown, K. H.; Dickinson, P. A.; Ghiorghiu, S.; Ranson, M. AZD9291 in EGFR Inhibitor Resistant Non Small-Cell Lung Cancer. *N. Engl. J. Med.* **2015**, *372*, 1689-1699.
32. Finlay, M. R. V.; Anderton, M.; Ashton, S.; Ballard, P.; Bethel, P. A.; Box, M. R.; Bradbury, R. H.; Brown, S. J.; Butterworth, S.; Campbell, A.; Chorley, C.; Colclough, N.; Cross, D. A. E.; Currie, G. S.; Grist, M.; Hassall, L.; Hill, G. B.; James, D.; James, M.; Kemmitt, P.; Klinowska, T.; Lamont, G.; Lamont, S. G.; Martin, N.; McFarland, H. L.; Mellor, M. J.; Orme, J. P.; Perkins, D.; Perkins, P.; Richmond, G.; Smith, P.; Ward, R. A.; Waring, M. J.; Whittaker, D.; Wells, S.; Wrigley, G. L. Discovery of a Potent and Selective EGFR Inhibitor (AZD9291) of

Both Sensitizing and T790M Resistance Mutations That Spares the Wild Type Form of the Receptor. *Journal of Medicinal Chemistry* 57, 8249-8267.

33. Walter, A. O.; Sjin, R. T. T.; Haringsma, H. J.; Ohashi, K.; Sun, J.; Lee, K.; Dubrovskiy, A.; Labenski, M.; Zhu, Z.; Wang, Z.; Sheets, M.; Martin, T. S.; Karp, R.; van Kalken, D.; Chaturvedi, P.; Niu, D.; Nacht, M.; Petter, R. C.; Westlin, W.; Lin, K.; Jaw-Tsai, S.; Raponi, M.; Dyke, T. V.; Etter, J.; Weaver, Z.; Pao, W.; Singh, J.; Simmons, A. D.; Harding, T. C.; Allen, A. Discovery of a mutant-selective covalent inhibitor of EGFR that overcomes T790M-mediated resistance in NSCLC. *Cancer discovery* 3, 1404-1415.

34. Thress, K. S.; Paweletz, C. P.; Felip, E.; Cho, B. C.; Stetson, D.; Dougherty, B.; Lai, Z.; Markovets, A.; Vivancos, A.; Kuang, Y.; Ercan, D.; Matthews, S. E.; Cantarini, M.; Barrett, J. C.; Janne, P. A.; Oxnard, G. R. Acquired EGFR C797S mutation mediates resistance to AZD9291 in non-small cell lung cancer harboring EGFR T790M. *Nat. Med.* advance online publication.

35. Yu, H. A.; Tian, S. K.; Drilon, A. E.; Borsu, L.; Riely, G. J.; Arcila, M. E.; Ladanyi, M. Acquired Resistance of EGFR-Mutant Lung Cancer to a T790M-Specific EGFR Inhibitor: Emergence of a Third Mutation (C797S) in the EGFR Tyrosine Kinase Domain. *JAMA Oncology* 2015, Published Online: May 7, 2015. doi:10.1001/jamaoncol.2015.1066.

36. Niederst, M. J.; Hu, H.; Mulvey, H. E.; Lockerman, E. L.; Garcia, A. R.; Piotrowska, Z.; Sequist, L. V.; Engelman, J. A. The allelic context of the C797S mutation acquired upon treatment with third generation EGFR inhibitors impacts sensitivity to subsequent treatment strategies. *Clinical Cancer Research* 2015, doi:10.1158/1078-0432.CCR-15-0560

37. [http://www.ariad.com/pdf/Rivera\\_2012\\_AACR\\_POSTER\\_AP26113\\_noQRcode.pdf](http://www.ariad.com/pdf/Rivera_2012_AACR_POSTER_AP26113_noQRcode.pdf)

38. <http://www.ariad.com/AP26113>

39. Hanan, E. J.; Eigenbrot, C.; Bryan, M. C.; Burdick, D. J.; Chan, B. K.; Chen, Y.; Dotson, J.; Heald, R. A.; Jackson, P. S.; La, H.; Lainchbury, M. D.; Malek, S.; Purkey, H. E.; Schaefer, G.; Schmidt, S.; Seward, E. M.; Sideris, S.; Tam, C.; Wang, S.; Yeap, S. K.; Yen, I.; Yin, J.; Yu, C.; Zilberleyb, I.; Heffron, T. P. Discovery of Selective and Noncovalent Diaminopyrimidine-Based Inhibitors of Epidermal Growth Factor Receptor Containing the T790M Resistance Mutation. *J. Med. Chem.* 2014, 57, 10176-10191.

40. Bissantz, C.; Kuhn, B.; Stahl, M. A medicinal chemist's guide to molecular interactions. *J. Med. Chem.* 2010, 53, 5061-84.

41. A total of 34 out of 531 (6%) kinases have equivalent Met + Thr residues and 27 out of 531 (5%) kinases have equivalent Met + Ser residues.

42. Hughes, J. D. B., J.; Price, D.A.; Bailey, S.; Decrescenzo, G.A.; Devraj, R.V.; Ellsworth, E.; Fobian, Y.M.; Gibbs, M.E.; Gilles, R.W.; Greene, N.; Huang, E.; Krieger-Burke, T.; Loesel, J.; Wager, T.; Whiteley, L.; Zhang, Y. Physicochemical drug properties associated with in vivo toxicological outcomes. *Bioorg. Med. Chem. Lett.* 2008, 18, 4872-4875.

43. Leeson, P. D.; Springthorpe, B. The influence of drug-like concepts on decision-making in medicinal chemistry. *Nat. Rev. Drug Discovery* 2007, 6, 881-890.

44. Lovering, F.; Bikker, J.; Humblet, C. Escape from Flatland: Increasing Saturation as an Approach to Improving Clinical Success. *J. Med. Chem.* 2009, 52, 6752-6756.

45. Ritchie, T. J.; Macdonald, S. J. The impact of aromatic ring count on compound developability: further insights by examining carbo- and hetero-aromatic and -aliphatic ring types. *Drug Discov. Today* 2011, 16, 164-171.

- 1  
2  
3 46. Lee, H. J.; Schaefer, G.; Heffron, T. P.; Shao, L.; Ye, X.; Sideris, S.; Malek, S.; Chan, E.;  
4 Merchant, M.; La, H.; Ubhayakar, S.; Yauch, R. L.; Pirazzoli, V.; Politi, K.; Settleman, J.  
5 Noncovalent wild-type-sparing inhibitors of EGFR T790M. *Cancer Discov* **2013**, *3*, 168-81.  
6 47. Shultz, M. D. Setting expectations in molecular optimizations: Strengths and limitations  
7 of commonly used composite parameters. *Bioorg. Med. Chem. Lett.* **2013**, *23*, 5980–5991.  
8 48. Tarcsay, Á.; Nyíri, K.; Keserü, G. M. Impact of Lipophilic Efficiency on Compound  
9 Quality. *J. Med. Chem.* **2012**, *55*, 1252-1260.  
10 49. Shultz, M. D. Improving the Plausibility of Success with Inefficient Metrics. *ACS Med.*  
11 *Chem. Lett.* **2013**, *5*, 2-5.  
12 50. Hopkins, A. L.; Keserü, G. M.; Leeson, P. D.; Rees, D. C.; Reynolds, C. H. The role of  
13 ligand efficiency metrics in drug discovery. *Nat. Rev. Drug Discovery* **2014**, *13*, 105-121.  
14 51. Shultz, M. D. The thermodynamic basis for the use of lipophilic efficiency (LipE) in  
15 enthalpic optimizations. *Bioorg. Med. Chem. Lett.* **2013**, *23*, 5992–6000.  
16 52. Pryde, D. C.; Dalvie, D.; Hu, Q.; Jones, P.; Obach, R. S.; Tran, T.-D. Aldehyde Oxidase:  
17 An Enzyme of Emerging Importance in Drug Discovery. *J. Med. Chem.* **2010**, *53*, 8441-8460.  
18 53. in vitro rat hepatocyte predicted clearance 35 mL/min/kg, in vivo plasma clearance 40  
19 mL/min/kg  
20 54. Measured pKa for 15 was 6.4 indicating that it is unlikely that any of these compounds  
21 are significantly ionized at pH7.4.  
22 55. <http://www.chem.wisc.edu/areas/reich/handouts/a-values/a-values.htm>.  
23 56. cLogP < 4.0, aromatic rings < 4, solubility index < 7.0, cHLM\_prob > 0.2, MW < 450,  
24 rotatable bonds < 8, also removed everything with no H-bonding potential.  
25 57. Blocking of the pyrimidine C4 and C5 positions with substituents results in loss of  
26 TMLR potency (data not shown).  
27 58. van Niel M. B.; Collins, I. B., M. S.; Broughton, H.; Cheng, S. K. F.; Goodacre, S. C.;  
28 Heald, A.; Locker, K.; MacLeod, A. M.; Morrison, D.; Moyes, C. R.; O'Connor, D.; Pike, A.;  
29 Rowley, M.; Russell, M.G.N; Sohal, B.; Stanton, J. ; Thomas, S.; Verrier, H.; Watt, A. P.;  
30 Castro. J. L. Fluorination of 3-(3-(Piperidin-1-yl)propyl)indoles and 3-(3-(Piperazin-1-  
31 yl)propyl)indoles Gives Selective Human 5-HT1D Receptor Ligands with Improved  
32 Pharmacokinetic Profiles. *J. Med. Chem.* **1999**, *42*, 2087-2104.  
33 59. Müller, K.; Faeh, C.; Diederich, F. Fluorine in pharmaceuticals: looking beyond intuition.  
34 *Science* **2007**, *317*, 1881-6.  
35 60. Vulpetti, A.; Dalvit, C. Fluorine local environment: from screening to drug design. *Drug*  
36 *Discov. Today* **2012**, *17*, 890-7.  
37 61. Rosenberg, R. E. Does fluoromethane form a hydrogen bond with water? *J. Phys. Chem.*  
38 *A* **2012**, *116*, 10842-9.  
39 62. Giuffredi, G. T.; Gouverneur, V.; Bernet, B. Intramolecular OH...FC Hydrogen Bonding  
40 in Fluorinated Carbohydrates: CHF is a Better Hydrogen Bond Acceptor than CF2. *Angew.*  
41 *Chem., Int. Ed.* **2013**, *52*, 10524-10528.  
42 63. Meanwell, N. A. Synopsis of some recent tactical application of bioisosteres in drug  
43 design. *J. Med. Chem.* **2011**, *54*, 2529-91.  
44 64. Böhm, H. J.; Banner, D.; Bendels, S.; Kansy, M.; Kuhn, B.; Müller, K.; Obst-Sander, U.;  
45 Stahl, M. Fluorine in Medicinal Chemistry. *ChemBioChem* **2004**, *5*, 637-643.  
46 65. Sun, A.; Lankin, D. C.; Hardcastle, K.; Snyder, J. P. 3-Fluoropiperidines and N-methyl-3-  
47 fluoropiperidinium salts: the persistence of axial fluorine. *Chemistry* **2005**, *11*, 1579-91.  
48 66. Rat microsomal/hepatocyte clearance data mL/min/kg: 34 = 18/20 35 = 12/11 36 = 13/13.  
49  
50  
51  
52  
53  
54  
55  
56  
57  
58  
59  
60

- 1  
2  
3 67. Zürcher, M.; Diederich, F. Structure-based drug design: exploring the proper filling of  
4 apolar pockets at enzyme active sites. *J. Org. Chem.* **2008**, *73*, 4345-61.
- 5 68. Poulin, P.; Hop, C. E.; Ho, Q.; Halladay, J. S.; Haddad, S.; Kenney, J. R. Comparative  
6 Assessment of In Vitro–In Vivo Extrapolation Methods used for Predicting Hepatic Metabolic  
7 Clearance of Drugs. *J. Pharm. Sci.* **2012**, *101*, 4308-4326.
- 8 69. Clearance in excess of liver blood flow was observed in mice for 42a and 42b, see  
9 Supporting Information page S10.
- 10 70. Lee, H.-J.; Schaefer, G.; Heffron, T. P.; Shao, L.; Ye, X.; Sideris, S.; Malek, S.; Chan, E.;  
11 Merchant, M.; La, H.; Ubhayakar, S.; Yauch, R. L.; Pirazzoli, V.; Politi, K.; Settleman, J.  
12 Noncovalent Wild-type–Sparing Inhibitors of EGFR T790M. *Cancer Discovery* **2013**, *3*, 168-  
13 181.
- 14 71. Halladay, J. S.; Wong, S.; Jaffer, S. M.; Sinhababu, A. K.; Khojasteh-Bakht, S. C.  
15 Metabolic Stability Screen for Drug Discovery Using Cassette Analysis and Column Switching.  
16 *Drug Metab. Lett.* **2014**, *1*, 67-72.
- 17 72. Ndubaku, C. O.; Heffron, T. P.; Staben, S. T.; Baumgardner, M.; Blaquiére, N.; Bradley,  
18 E.; Bull, R.; Do, S.; Dotson, J.; Dudley, D.; Edgar, K. A.; Friedman, L. S.; Goldsmith, R.; Heald,  
19 R. A.; Kolesnikov, A.; Lee, L.; Lewis, C.; Nannini, M.; Nonomiya, J.; Pang, J.; Price, S.; Prior,  
20 W. W.; Salphati, L.; Sideris, S.; Wallin, J. J.; Wang, L.; Wei, B.; Sampath, D.; Olivero, A. G.  
21 Discovery of 2- $\{3-[2-(1\text{-Isopropyl-3-methyl-1H-1,2,4-triazol-5-yl})-5,6-$   
22  $\text{dihydrobenzo}[f]\text{imidazo}[1,2-d][1,4]\text{oxazepin-9-yl}]$ -1H-pyrazol-1-yl $\}$ -2-methylpropanamide  
23 (GDC-0032): A  $\beta$ -Sparing Phosphoinositide 3-Kinase Inhibitor with High Unbound Exposure  
24 and Robust in Vivo Antitumor Activity. *J. Med. Chem.* **2013**, *56*, 4597-4610.
- 25 73. Eigenbrot, C.; Stamos, J.; Sliwkowski, M., X. . Structure of the Epidermal Growth Factor  
26 Receptor Kinase Domain Alone and in Complex with a 4-Anilinoquinazoline Inhibitor. *J. Bio.*  
27 *Chem.* **2002**, *277*, 46265-46272.
- 28  
29  
30  
31  
32  
33  
34  
35  
36  
37  
38  
39  
40  
41  
42  
43  
44  
45  
46  
47  
48  
49  
50  
51  
52  
53  
54  
55  
56  
57  
58  
59  
60